An Improved Charged Particle Track Reconstruction Algorithm for the Micromegas Detectors of the New Small Wheel for the ATLAS Experiment at the Large Hadron Collider

Citation	Satterthwaite, Thomas Peabody. 2021. An Improved Charged Particle Track Reconstruction Algorithm for the Micromegas Detectors of the New Small Wheel for the ATLAS Experiment at the Large Hadron Collider. Bachelor's thesis, Harvard College.
Citable link	https://nrs.harvard.edu/URN-3:HUL.INSTREPOS:37368571
Terms of Use	This article was downloaded from Harvard University's DASH repository, and is made available under the terms and conditions applicable to Other Posted Material, as set forth at http://nrs.harvard.edu/urn-3:HUL.InstRepos:dash.current.terms-of-use#LAA

An Improved Charged Particle Track Reconstruction Algorithm for the Micromegas Detectors of the New Small Wheel for the ATLAS Experiment at the Large Hadron Collider

A THESIS PRESENTED
BY
THOMAS PEABODY SATTERTHWAITE
TO
THE DEPARTMENT OF PHYSICS
AND TO
THE DEPARTMENT OF COMPUTER SCIENCE

IN PARTIAL FULFILLMENT OF THE REQUIREMENTS
FOR THE DEGREE OF
BACHELOR OF ARTS
IN THE SUBJECTS OF
PHYSICS AND COMPUTER SCIENCE

HARVARD UNIVERSITY
CAMBRIDGE, MASSACHUSETTS
MARCH 2021

Thesis advisor: Professor Melissa Franklin Thomas Peabody Satterthwaite

An Improved Charged Particle Track Reconstruction Algorithm for the Micromegas Detectors of the New Small Wheel for the ATLAS Experiment at the Large Hadron Collider

Abstract

The forthcoming High-Luminosity Large Hadron Collider upgrade brings potential for the discovery of new physics. However, the HL-LHC also brings new technological challenges as the Collider increases its luminosity beyond its intended value. As the number of collisions increases, so too does the hit rate in the ATLAS Experiment's muon spectrometer. To tackle this challenge, the New Small Wheel is being commissioned to provide a dedicated trigger and precision tracker to the end-cap region of the ATLAS Experiment's muon system. Two technologies: small-strip thin gap chambers (sTGCs) and micro-mesh gaseous structures (micromegas) provide these triggering and tracking capabilities, respectively. Before the micromegas are installed, they are tested at CERN using cosmic ray muons. This requires an efficient set of data analysis tools so that the detector's performance can be evaluated.

This thesis presents a set of algorithms which are used to determine that these detectors work and how well they work. A divide-and-conquer approach yields an efficient algorithm for locating tracks of charged particles in micromegas detector data. The parameters which describe each charged particle's trajectory can then be fit to the data in linear time using an analytical solution to

χ^2 minimization. Analyzing the Hessian matrix of this χ^2 function also allows for improved bounds to be placed on the micromegas detector's precision. This removes poor-quality tracks from detector data, and it helps ensure that the detectors are satisfying the requirements set forth in the New Small Wheel's Technical Design Report. A discussion of the track identification algorithm's utility in disappearing-track-based searches for long-lived supersymmetric particles is also presented.

Contents

Listing of figures

Listing of tables

Acknowledgments

THANK YOU to the members of the Harvard ATLAS Group and to the members of the New Small Wheel team for their guidance throughout this project. Thank you especially to Professor Melissa Franklin, Professor Theodoros Alexopoulos, Dr. Alex Tuna, Dr. Larry Lee, Ann Wang, Gabriel Rabanal-Bolaños, Anne Fortman, and Jerry Ling, with whom I worked most closely. Thank you also to the faculty members at Harvard and beyond who have shaped my undergraduate career.

1

Introduction

1.1 LARGE HADRON COLLIDER

The Large Hadron Collider was commissioned in 2008 with the goal of discovering new physics[15]. One hundred meters below the surface of Geneva, Switzerland, the Large Hadron Collider (LHC) collides particles at close to the speed of light and uses the products of these collisions to learn about the nature of matter at the high energy frontier[13]. In 2012, physicists at CERN, the organization

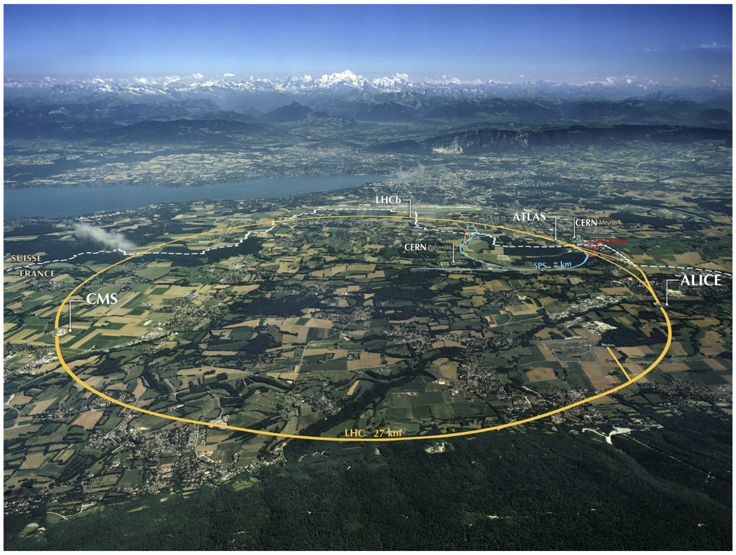

Figure 1.1: Aerial view of the Swiss-French border with the position of the LHC and its experiments shown. Source: CERN[8].

which operates the LHC, used Collider data to report one of the largest scientific breakthroughs of the century: the production of the Higgs boson[2]. This landmark discovery, which was confirmed by the detection of the Higgs boson's decay products, gave experimental evidence for a decades-old theory which explains the fundamental conundrum of how elementary particles get mass[20]. Despite this monumental success, however, many questions about the fundamental nature of our universe remain unanswered by current data from the LHC.

The Standard Model of particle physics is the theory which describes the processes that have thus far been observed in LHC collisions[18]. The vast amount of data collected by experiments at the LHC make the Standard Model one of the most successful theories in all of physics[13]. In spite of this success, however, many mysteries still loom over the field. For example, physicists are not able to explain the nature of the dark matter which makes up the vast majority of our universe[26], nor can they reconcile how general relativity, Einstein's theory of gravity, works on the universe's smallest scales[35]. Therefore, the Standard Model must be amended. Before it can be fixed, however, it must first be broken[10].

Given that present experiments at the Large Hadron Collider have only confirmed the Standard Model's predictions, the production of phenomena which is not explained by the Model must be exceedingly rare. To increase the likelihood of observing physics which goes beyond the Standard Model (BSM), then, more collisions must be observed[7]. This motivates the High-Luminosity Large Hadron Collider (HL-LHC), an upgrade to the current LHC which aims to come online in 2027[12]. The Collider's luminosity, the number of particles it collides, will be increased by roughly five times so that more proton-proton (*pp*) collisions can be observed by experiments around the LHC[14]. Buried in the decay products of these collisions, physicists hope to find evidence for BSM phenomena[14].

An upgraded Large Hadron Collider, operating at a luminosity much higher than originally intended, requires an upgraded set of tools for handling the new deluge of particles[23]. Particle accelerators must cope with many sources of background processes that must be filtered out when searching for interesting phenomena. The LHC's beam of particles, for example, is likely to interact with the beam pipe's material as it circumnavigates the Collider at close to the speed of light. This generates a beam halo which interacts with detectors[32]. Collimated showers of particles, known as jets, which are produced by *pp*-collisions can also interact with detector material and produce free neutrons. As these neutrons scatter, they can be read out by detectors and produce cavern background[17]. These events will only become more frequent as the LHC's luminosity is increased. They

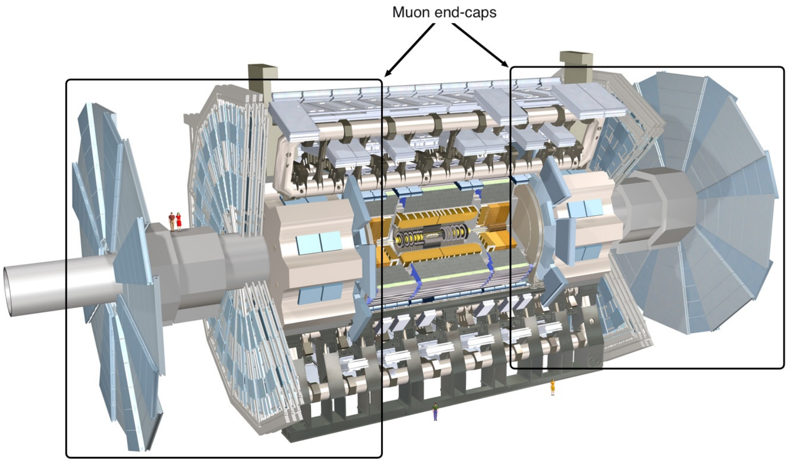

Figure 1.2: Schematic of the ATLAS Experiment with the end-cap regions of the muon system highlighted. Source: CERN[29].

will degrade existing detectors, and generate a large amount of undesirable data[23].

1.2 ATLAS Muon System

These background processes pose a significant challenge to the muon system of the ATLAS Experiment. The ATLAS (A Toroidal LHC Apparatus) Experiment, shown in figure 1.2, provides a large, general-purpose set of detectors which surrounds one of the Large Hadron Collider's points of collisions[4]. Using a range of technologies, the ATLAS Experiment seeks to measure the energies and trajectories of each of the different types of particles which can be produced by a *pp*-collision. The muon, which is akin to a heavy electron, is one of these particles. The relatively high mass and long lifetime of the muon allow it to travel deeper into the detector than many of the other particles produced by a *pp*-collision[18]. The end-cap region of the Experiment, which provides muon detectors

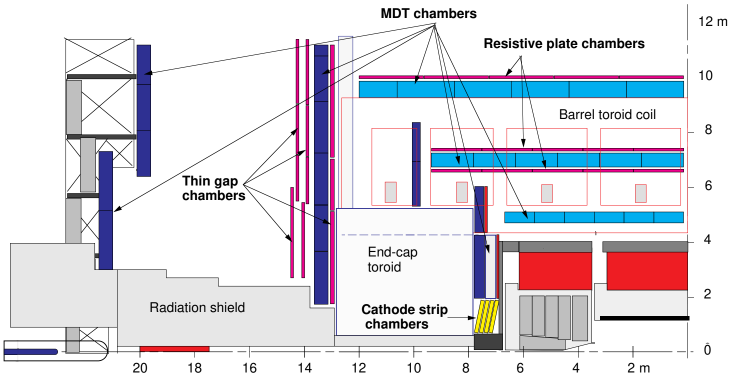

Figure 1.3: Diagram of the ATLAS Experiment's muon system, with the end-cap region shown in indigo. Interaction point shown in the bottom right-hand corner. Muons travel right to left. Source: ATLAS Collaboration[5].

to cover $1.0 < |\eta| < 2.7$[23] (polar angle along the beam pipe between 7.7° and 40.4°), is vital for tracking these particles. Following the forthcoming upgrade to the HL-LHC, this region of the Experiment will be particularly susceptible to degrading radiation and background events[23]. It must be prepared for the new challenges which lie ahead.

A schematic of this muon system is shown in figure 1.3. The end-cap region, shown in indigo, uses successive layers of monitored drift tubes (MDTs) to determine the trajectories of incident muons[4]. These MDTs confine a gas around a wire which can read out a charge to front-end electronics. As a muon passes through the tube, it ionizes the gas and generates an electric charge which accumulates on the wire[24]. By placing layers of MDTs before and after a magnetic field, which is produced by the end-cap toroid, the muon's momentum can be determined. Lower momentum charged particles will curve less in the magnetic field[31]. Therefore, matching muon tracks in successive layers of MDTs show how much the track was deflected by the magnetic field, which tells of the particle's momentum[4].

Thin gap chambers (TGCs) are also used to ensure that the MDTs only record data from real muons with a sufficiently high momentum[4]. These detectors have a shorter drift time, which allows them to detect the presence of incident charged particles faster than the MDTs[27]. By placing a layer of TGCs prior to each layer of MDTs, the TGCs can serve as triggers. Requiring that tracks in the MDTs coincide with signals from the TGCs ensures that recorded data only contains muons of a sufficiently high momentum[17]. Using these two technologies in tandem, a trigger (TGC) and a tracker (MDT) allow the ATLAS Experiment's muon system to resolve the momenta and trajectories of real muons.

These MDTs and TGCs are, of course, subject to the aforementioned background processes. The beam halo and cavern background lead to a large number of hits in the MDTs, even with the presence of the TGC triggers[23]. As the electrons produced by these particles in the ionized gas of the MDTs drift towards the readout wires, the MDTs are effectively offline for several *pp*-collisions before they are ready to detect muons again. This reduces the Experiment's sensitivity to interesting phenomena, and this issue is only expected to worsen in the era of the HL-LHC[23]. To help resolve this issue, the ATLAS Experiment is commissioning the New Small Wheel. This new detector will replace the first set of TGCs and MDTs of the muon system's end-cap, as shown in figure 2.1. Using two new technologies, the New Small Wheel will be able to resolve the trajectories of high momentum muons without being as influenced by beam halos or cavern background[23].

To provide a more robust trigger, the TGCs are being replaced by small-strip thin gap chambers (sTGCs). The narrower strips of these detectors as compared to the TGCs will provide better position and timing resolution[23]. Furthermore, the presence of four layers of these detectors in series will allow for a coincidence requirement to help discriminate against background processes[23]. To provide a more precise tracker, the MDTs are being replaced by micro-mesh gaseous structures (micromegas). These detectors use a stronger electric field to decrease the drift time of ionized electrons[23]. Therefore, should a rogue particle create a signal in a micromegas detector, the detector will not be incapacitated for as long.

1.3 Contributions

As the New Small Wheel is prepared for installation to the ATLAS Experiment, these sTGCs and micromegas must be constructed and tested. Tests of the micromegas detectors have been carried out in building BB5 of CERN's campus in Geneva, Switzerland to ensure that they operate as expected and provide the desired precision[23]. Cosmic rays, which are showers of particles of extraterrestrial origin, provide an ever-present source of sufficiently high energy muons with which to test the micromegas detectors[18]. On the order of 10^3 of these muons pass through the fiducial region of a wedge of micromegas detectors each second[35], creating a vast amount of data during test runs.

Sifting through and analyzing the data that these tests produce in a computationally efficient manner, however, poses a daunting challenge. In this thesis, I present a set of novel algorithms to efficiently identify tracks of muons in micromegas detector data, and to statistically fit the parameters which describe these particles' tracks to the data. Using a divide-and-conquer approach yields an efficient algorithm for identifying tracks of particles. In practice, this gives a 36x improvement to the speed of track identification when compared to the previous brute force solution. This allows for more data to be analyzed in a radically shorter amount of time. Using an analytical solution for the minimum value of the χ^2 goodness of fit test for the parameters which describe a particle's trajectory through the micromegas detectors then allows for these parameters to be fit in linear time. This provides a more robust method for describing the particle's trajectory, and it motivates an important metric for understanding the precision of the micromegas detectors. This is critical for ensuring that the detectors are meeting the precision requirements set forth in the New Small Wheel's Technical Design Report[23], and for removing poor-quality tracks from the detectors' data.

The divide-and-conquer nature of the particle track identification algorithm also allows it to identify tracks of particles which only appear in a subset of the detector's layers. If extended to a larger region of the ATLAS Experiment, this technique could be used to locate tracks of particles which only pass through a subset of the Experiment's detectors. Such a particle track could be used in studies which search for the production of long-lived supersymmetric particles in data from the LHC. Discovery of such a particle would disrupt particle physics as it would give experimental evidence for a phenomenon which transcends what is currently described by the Standard Model[1].

This thesis is organized as follows. In chapter 2, I describe the layout of the New Small Wheel and its layers of sTGC and micromegas detectors. In chapter 3, I present the algorithm for identifying a charged particle's track through the micromegas detectors. In chapter 4, I present the improved method for statistically fitting the parameters which describe these particle tracks to detector data, as well as a discussion of its implications for evaluating the detector's precision. Finally, in appendix C, I discuss the utility of the track identification algorithm in searching for long-lived supersymmetric particles. A conclusion is presented in chapter 5.

2

New Small Wheel

2.1 Overview

The ATLAS Experiment provides a general-purpose detector with 4π steradian coverage surrounding an interaction point at the Large Hadron Collider[17]. Several layers of calorimeters and semiconductor- and gas-based tracking detectors seek to provide measurements of the energies and

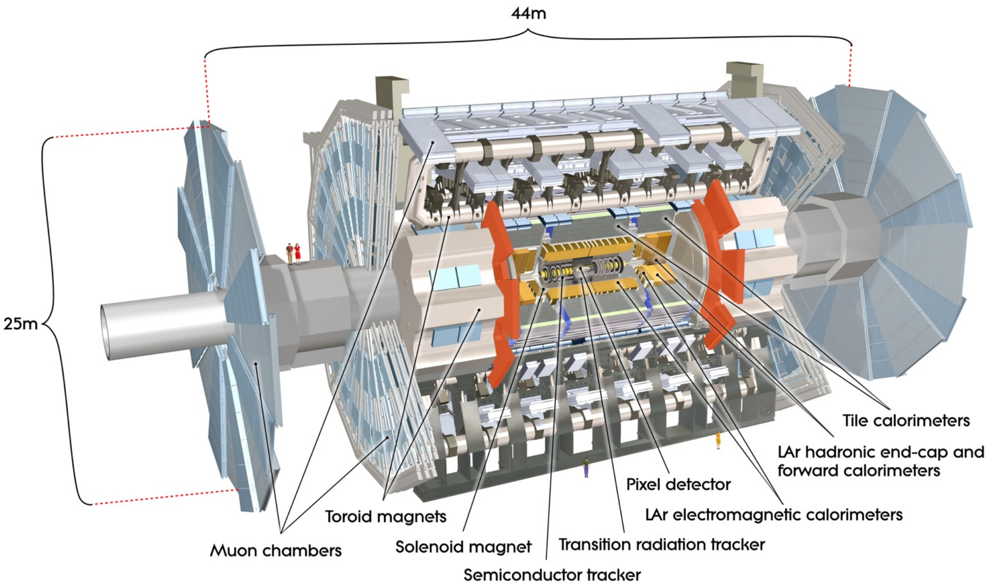

Figure 2.1: Diagram of the ATLAS Experiment with the positions of the New Small Wheels highlighted in red. Source: CERN[29].

trajectories of each of the particles which could be produced by a proton-proton collision[4]. Full coverage in solid angle around the interaction point makes the ATLAS Experiment a hermetic detector, and this gives the Experiment a high probability of detecting a particle regardless of its trajectory[17]. This general-purpose nature makes the Experiment very well suited to discovering new physics without bias towards existing theories[4].

As the ATLAS Experiment prepares for the LHC's upcoming run of data collection and for the HL-LHC, the New Small Wheel is being commissioned during phase one of the Experiment's upgrades[21]. The effects of the beam halo and of cavern background mean that the increased luminosity of the LHC will cause more degradation to and decreased performance of the existing thin gap chambers and monitored drift tubes which are currently used in the Experiment's muon sys-

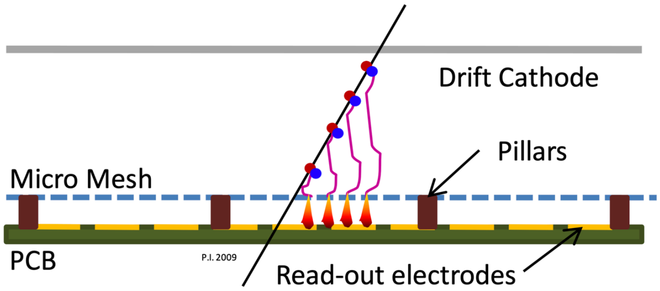

Figure 2.2: Diagram showing how micromegas technology detects an ionizing particle. Source: ATLAS Collaboration[23].

tem[23]. This manifests in detectors which have a shorter lifetime, and in reconstructed tracks of particles which may not have originated from real muons. The New Small Wheel will cope with these challenges by using two technologies, small-strip thin gap chambers (sTGCs) and micro-mesh gaseous structures (micromegas), in series. The sTGCs will provide a more robust trigger, while the micromegas will be better suited to higher fluxes of incident particles due to their fast evacuation time[23]. Once installed to the end-cap region of the Experiment's muon system, as shown in figure 2.1, these capabilities of the detector will allow it to provide a significant contribution to the ATLAS Experiment's search for new physics[23].

The New Small Wheel contains eight layers each of sTGC and micromegas detectors. These detectors are arranged along the z-dimension as four layers of sTGCs, eight layers of micromegas, and a final four layers of sTGCs. A coincidence requirement on the sTGCs allow for these layers to serve as a trigger for the tracking micromegas layers. These detectors are constructed in wedges with 16 wedges used to cover ϕ when arranged around the beam pipe[23] like slices of a cake, as shown in figures 2.3 and 2.6. Unlike slices of a cake, however, these wedges are explicitly designed to overlap one another so that there is no non-fiducial region in the detector[23].

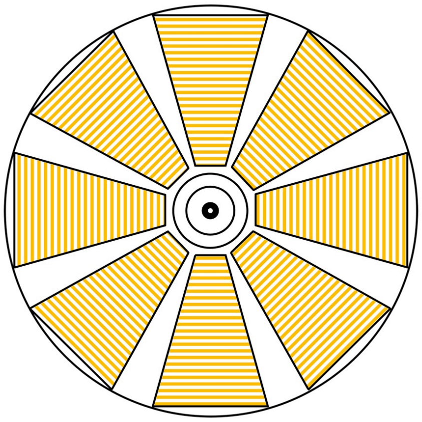

Figure 2.3: Diagram showing how eight micromegas wedges surround the beam pipe on the New Small Wheel. Eight more wedges are used to cover the bare regions. Strips of an η layer are shown. Strips not drawn to scale.

2.2 Micromegas Detectors

The subject of this thesis is the micromegas detectors. These detectors work by confining a gaseous mixture between two charged plates which create an electrostatic potential[16]. As shown in figure 2.2, a charged particle (i.e. muon) ionizes this gas and causes a shower of electrons to travel along the potential to a micro-mesh. At this point, a stronger electric field amplifies the charge so that it can be read out along one or a number of adjacent copper strips as an electric signal and processed by front-end electronics[16]. These strips are arranged radially outward from the beam pipe, as shown in figure 2.3, so that a precise measurement of a particle's position can be made in η at each layer[23]. Locally, in New Small Wheel coordinates, this corresponds to making a measurement in the x-direction.

It is also desirable that a measurement be made in ϕ. This is achieved by offsetting the strips of four of the eight micromegas layers by an angle of $\pm 1.5°$, two layers in either direction, as shown in

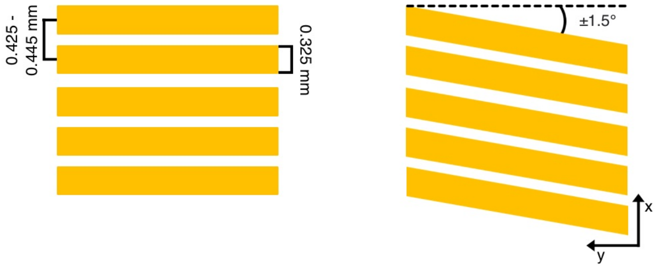

Figure 2.4: Diagram showing how stereo layer readout strips (right) are offset from those of the η layers (left). Angle not shown to scale.

figure 2.4[23]. These four layers are dubbed the ‘stereo’ layers, and they allow for an imprecise measurement to be made in ϕ. Considering the overlap of consecutive strips which are oriented at a non-trivial angle with respect to one another allows for a measurement to be made of an incident particle’s trajectory in both η and ϕ[23]. A cartoon diagram of this is shown in figure 2.5. Locally, in New Small Wheel coordinates, this ϕ measurement corresponds to the y-direction. It should be noted, however, that strips along the η layers of micromegas detectors are not curved to follow a constant η value. Use of the stereo layers is, therefore, imperative in order to pinpoint a y value and, by extension, determine the η value of a trajectory.

We then have eight micromegas layers which are used to determine the trajectory of a muon. Four η layers produce measurements only in x while four stereo layers also produce measurements in y. Using these local New Small Wheel coordinates, we will refer to the four η layers as ‘X’ layers. To distinguish between the two types of stereo layers, we define ‘U’ layers to be those whose strips are offset by an angle of $+1.5°$ and we define ‘V’ layers to be those whose strips are offset by $-1.5°$. The layer structure of each micromegas wedge, starting at the layer closest to the interaction point, is XXVUVUXX[23].

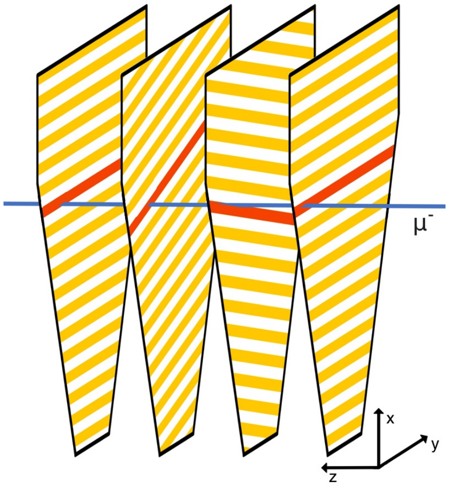

Figure 2.5: Diagram showing how an incident muon (blue) would be read out on strips (red) of several stacked η and stereo layers of micromegas detectors. Not drawn to scale.

2.3 COSMIC RAY TEST STAND

After construction, these wedges of micromegas detectors are tested in building BB5 of CERN's campus in Geneva, Switzerland prior to the New Small Wheel's installation to the ATLAS Experiment. Cosmic ray muons provide an ever-present stream of particles with which to evaluate the detector's performance; on the order of 10^3 cosmic muons pass through a micromegas wedge's fiducial region each second[35]. Runs of data collection at this cosmic ray test stand can last anywhere from seconds to hours. An efficient set of data analysis tools is therefore needed in order to turn individual strip readouts on micromegas layers into reconstructed charged particle trajectories through a wedge. A scintillator, which is placed above a wedge of micromegas detectors, is used to identify incident muons. This defines events and triggers data collection. Due to the effects of noise, identifying the straight line in each event which is indicative of the passage of a real muon becomes a non-trivial

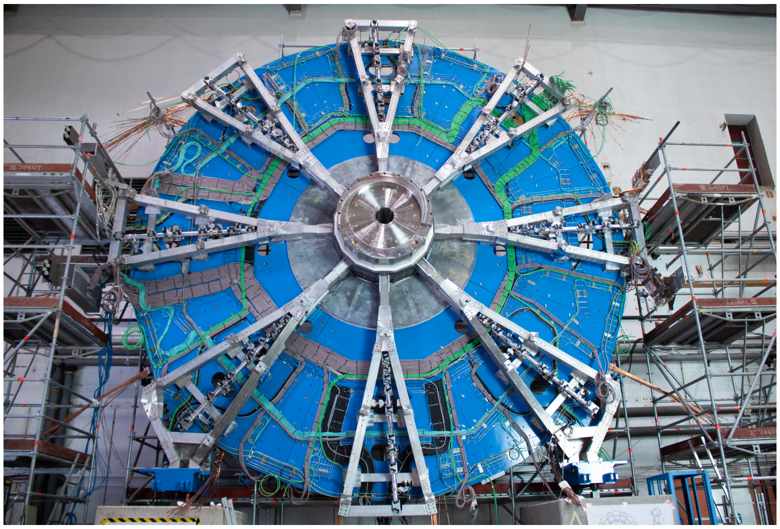

Figure 2.6: Photograph of the New Small Wheel's mechanical structure, without detector wedges installed. Source: CERN[34].

task. This pursuit therefore represents is a vital component of the cosmic ray test stand's data analysis efforts.

This event-level data analysis pipeline consists of several steps. During a muon's passage through a wedge, the ionizing particle's avalanche of electrons in the amplification region of a micromegas detector is likely to fire a number of adjacent readout strips[23]. These groups of strip hits on each layer are therefore condensed into single clusters for simplicity. A clustering algorithm groups hits together, with cluster centers defined by the weighted average of the positions of constituent hits, weighted by the electric charge on each strip. Once clusters have been identified, however, it is still likely that there are clusters which are noise amidst those which are signal. An algorithm must identify which clusters form a straight line, signaling a charged particle's track through the detector, and which do not. This algorithm is presented in the following chapter. Another algorithm must then statistically fit a straight line to these on-track clusters in the *xz* and *yz* planes so that statements can be made regarding the detector's precision as it tracks charged particles. This algorithm is presented in chapter 4.

3

Particle Track Identification

3.1 Algorithm Presentation

Having laid out the motivation for an algorithm which efficiently identifies tracks of charged particles in micromegas detector data, this algorithm may now be presented. The input of this algorithm is a set of cluster centers of fired readout strips from the eight layers of a micromegas wedge.

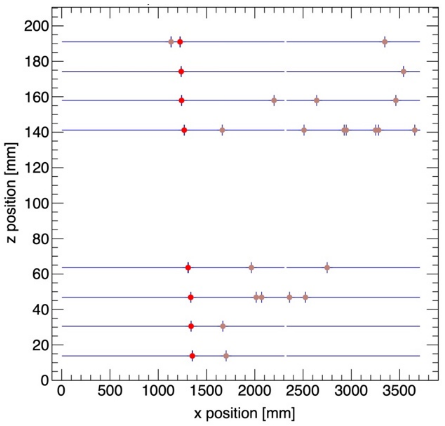

Figure 3.1: Sample event display of micromegas detector data from the cosmic ray test stand. Detector layer z positions shown as horizontal blue lines. Eight clusters which likely belong to a charged particle's track can be seen in red alongside twenty-one noise clusters shown in terracotta. Identifying these red clusters is the goal of the algorithm. Axes not to scale.

The output is a subset of these clusters which forms a straight line. As we will see, due to detector inefficiency and imprecision, it is desirable that this algorithm is able to identify tracks which appear on fewer than eight layers if no eight-layer tracks exist, and that it is able to identify tracks which are not perfectly straight.

This problem is distinct from the classic statistics problem of fitting a straight line to data. Whereas finding a line of best fit seeks to approximate a straight line to a cloud of an arbitrary number of data points, this algorithm seeks to identify a straight line buried in a sea of noise. Ideally, it should also be able to determine that no such line exists. Traditional methods such as linear regression are therefore not appropriate for this problem[19]. Statistically fitting the parameters of this straight line to the data will be discussed in the following chapter of this thesis. Presently, we are only concerned with determining if and where such a straight line exists.

To find a straight line in the three dimensions covered by a micromegas wedge, we can note several simplifications. Each detector layer is positioned at a constant z-value, so it is only necessary to search laterally along the strip readouts of these layers. Furthermore, it will not be necessary to identify more than one cluster per micromegas layer. Though it is expected that a single charged particle will be read out on multiple adjacent strips of a given layer, the clustering algorithm discussed in the previous chapter condenses these adjacent hits into single clusters[23]. Finally, the X layers provide a measurement in x only, with the y-coordinate left ambiguous as readout strips run parallel to the y-axis. For this track identification algorithm, we will also make the simplifying assumption that the offset angle of the stereo layers is 0° so that they can be treated as X layers as well. We will then use the x position of cluster centers at the center ($y = 0$) of the detector for these layers. This assumption will be justified shortly.

For now, let us also assume that the particle track appears on all eight layers of the detector. Pairing this with the aforementioned assumptions, it is clear to see that a particle track through the micromegas wedge also exists on a subset of its layers. Trivially, segments of a straight line are also straight. So, one could imagine finding a straight line of clusters on disjoint subsets of the detector's layers and attempting to stitch these lines together into the single line of a particle track. This insight empowers us to solve the problem using a divide-and-conquer approach. We can break the problem of finding an eight-layer track into first finding four separate two-layer tracks, with some extra overhead to combine them.

For the divide portion of the algorithm, we simply divide the eight layers of micromegas detectors into adjacent subsets; eight layers become two adjacent sets of four layers each. Each of these two subsets then becomes two adjacent sets of two layers each. Using zero-indexing, we have lay-

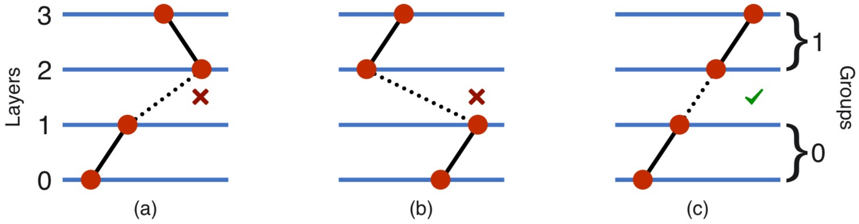

Figure 3.2: Illustration of how sub-tracks may be aligned or misaligned when recombining groups of layers. (a) Sub-tracks which are not well-aligned. (b) Sub-tracks which are well-aligned but do not connect nicely. (c) Sub-tracks which are well-aligned and which connect nicely.

ers zero and one, layers two and three, layers four and five, and layers six and seven. As a base case, within each of these four groups, we then consider all possible lines between combinations of clusters, where we pick one cluster on each layer. These are 'sub-tracks.' With a large amount of noise, we surely now have a number of sub-tracks which are meaningless alongside those which are not. We must discriminate to remove and condense sub-tracks as we recombine groups of layers.

During recombination, we seek to take two adjacent groups of layers and turn them into one group with straight tracks that have a cluster on each available layer. To achieve this, we will have to take each sub-track in one subset of layers and see if it connects to a sub-track in the other subset of layers. To filter out those which do not connect, the geometric angle between them is used as a measure of alignment. In the ideal scenario, the angle between two perfectly aligned sub-tracks corresponding to a single particle's track is $0°$. Of course, imperfect resolution of the detector and the effects of multiple scattering[35] make it unlikely for perfect alignment to occur. So, we will define an angle threshold as an upper limit on this alignment. Doing so allows us to filter out pairs of sub-tracks which are not well-aligned, as shown in figure 3.2a.

Two sub-tracks which are well-aligned may not nicely connect to one another if they appear offset in the detector, however. This case is illustrated in figure 3.2b. To also remove these pairs of sub-tracks, we must consider the line which connects the top cluster in the bottom group of layers to the bottom cluster in the top group of layers. The angle between this connecting line and the sub-track in either group must also satisfy the aforementioned threshold. Therefore, there are effectively three line segments being stitched into a single straight line, as shown in figure 3.2. It should also be noted that when stereo layers are involved in recombination, the angle threshold is increased by a constant factor. This accounts for how the angle of the strips on these layers offsets the strip readouts at large y values, and this factor should be set according to the maximum width of the wedge. Doing this allows us to justify approximating the stereo layers as X layers.

With all non-connecting sub-tracks removed, we are now left with sub-tracks which are well aligned and which connect nicely, as shown in figure 3.2c. Recombination can then proceed with two, now larger, groups of layers, using the exact same method to remove sub-tracks which do not connect further through the entire detector. In the end, we may be left with one or more straight lines of eight clusters, one on each layer, which are indicative of one or more particles' tracks through the micromegas wedge, as shown in figure 3.3. Alternatively, it is possible that no such line remains, which would indicate that a charged particle's track was not detected.

It should be noted that with an imprecise detector and a large alignment threshold, the identified line of clusters may zig-zag slightly as it traverses through the detector. Furthermore, this zig-zag may be present at intermediate stages of the algorithm's execution when there are, for example, just four clusters present and we seek to evaluate alignment with another sub-track. To avoid a computa-

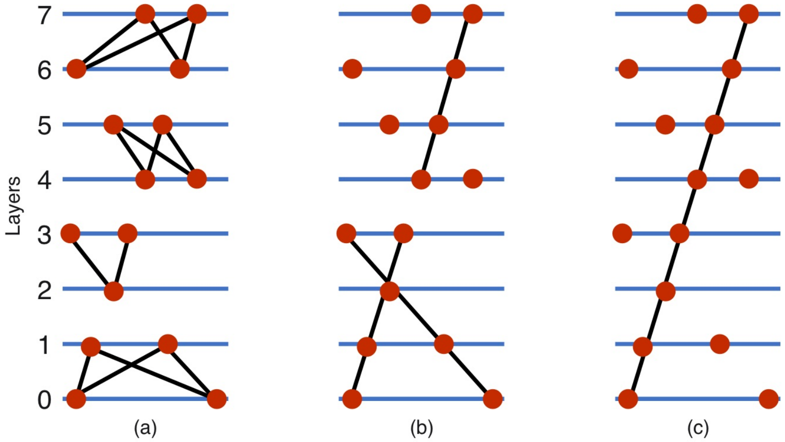

Figure 3.3: Illustration of how the algorithm finds an eight-cluster track in the presence of noise. Each step is presented: (a) base case, (b) sub-tracks which remain after one recombination, (c) the identified track.

tionally expensive search for the line of best fit to these data, the average vector is computed. That is, the displacement vector of consecutive pairs of clusters is calculated, using the z separation of those clusters as a weighting function. This estimates the 'average orientation' of a given sub-track, and it allows for future determinations to be made on how well two sub-tracks align.

3.2 CORRECTNESS AND EFFICIENCY

To see the correctness of this algorithm, we will proceed with a contradiction. Suppose that there is a straight track of eight clusters which is not identified by the algorithm. Segments of this track must have appeared in the base case where all possible sub-tracks were drawn. So, during some recombination, the alignment between two constituent sub-tracks must have exceeded the given threshold. For a perfectly straight line, however, this angle is 0°, which would be satisfied by any angular threshold. This therefore yields a contradiction. It should be noted, however, that the idea of correctness of this algorithm is rather fluid. In a real-world scenario, it is nearly impossible that any particle track will be identified with an alignment threshold of 0° due to the detector's imprecision, multiple scattering, and rounding errors. With a very imprecise detector, we may want to identify tracks which don't look terribly straight to the naked eye using a very large alignment threshold. The kind of track which the algorithm seeks to find can therefore be adjusted along with notions of what constitutes a track.

Much like the correctness of this algorithm, its efficiency is also dependent upon the nature of the micromegas wedge's data and the algorithm's angular threshold. In the event of a high angular threshold and data that is very tightly clustered in a small region of the detector, it is possible that no sub-tracks are removed during recombination. This leads to a large number of identified tracks; given n clusters in an event, which are reasonably well distributed across the detector's eight layers, this scenario would contain $\mathcal{O}(n^8)$ tracks. A bound of $\mathcal{O}(n^8)$ on the algorithm's run time can then be seen by analyzing its behavior. In the base case, $\mathcal{O}(n^2)$ sub-tracks are drawn. As these sub-tracks are evaluated for alignment and condensed, they become $\mathcal{O}(n^4)$ sub-tracks. These sub-tracks are then condensed further to $\mathcal{O}(n^8)$ final tracks. Evaluation of alignment at each recombination step is carried out using simple trigonometry, making this a constant time operation without any dependence on the number of clusters in the event. The same is true of recombination. The algorithm therefore runs in $\mathcal{O}(n^8)$ time. Clearly, this bound cannot be improved upon as each of the $\mathcal{O}(n^8)$ tracks in the event must be returned.

In practice, however, the angular threshold is smaller and the data is better distributed across the micromegas wedge. This leads to a significant improvement in the algorithm's speed as there are fewer tracks in each event. As sub-tracks are condensed, many which do not align with other sub-tracks are removed, and therefore do not need to be considered during future recombinations. Further improvements, such as the use of a hash table which is discussed below, also lead to a significant reduction in the number of sub-tracks which are considered for alignment during each step of recombination. This results in a dramatic improvement to the algorithm's run time when compared to that of the brute force algorithm. Previous solutions to this problem used a brute force approach which ran a χ^2 minimization on each of the $\mathcal{O}(n^8)$ potential tracks present in an event, and selected the track with the lowest χ^2. With high noise rates, this approach ground data analysis to a halt. Using micromegas data, this new algorithm identified tracks 36x faster than the brute force algorithm in data from a sample run of cosmic data collection at standard noise rates. It therefore represents a significant improvement to the cosmic ray test stand's data analysis tools.

3.3 Further Considerations

Given a sub-track and a maximum angle threshold, it is clear that a connecting sub-track in an adjacent group of layers can only be found in a narrow region of the detector. As a simple example, if a sub-track is pointing straight along the z-axis, then a connecting sub-track must lie directly above the first. We can then use the maximum angle threshold to define a search region for connecting sub-tracks in an adjacent group of layers. A diagram of this search region can be seen in figure 3.4. As shown in figure 3.4a, only the sub-tracks which lie in the orange search region are considered for alignment.

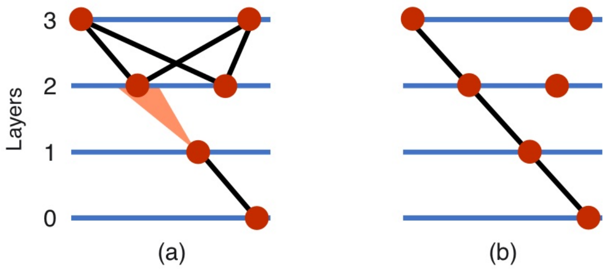

Figure 3.4: Illustration of how a search region is defined during recombination. When combining two groups of two layers each, (a) a search region for the bottom sub-track is established to find (b) a connecting sub-track.

This search region can be implemented using a simple hash table to store the sub-tracks during recombination. Hits in the micromegas detector are discretized by the non-trivial width of the strips which read out a charge. Each micromegas wedge has 8192 strips[23], so we will create 8192 bins in our hash table with collisions handled by a linked list. We will store each sub-track in this hash table using the index of the strip readout of its cluster on the lowest index layer, rounded to the nearest strip. Using simple trigonometry and the geometry of the detector, we can then calculate the index of the strip that a given sub-track points towards and look-up the corresponding sub-tracks in constant time. In order to account for imprecision, we will also look to the left and to the right of this identified strip to form a search region. The size of this region is proportional to the angular threshold, so this use of a hash table improves the efficiency of the algorithm by a factor which is inversely proportional to the alignment threshold.

Finally, as has been discussed, it is generally desirable that a particle track identification algorithm be able to identify tracks of particles which appear on a set of non-consecutive layers of the detector. Detector inefficiency means that that an incident particle may not be read out on all eight layers

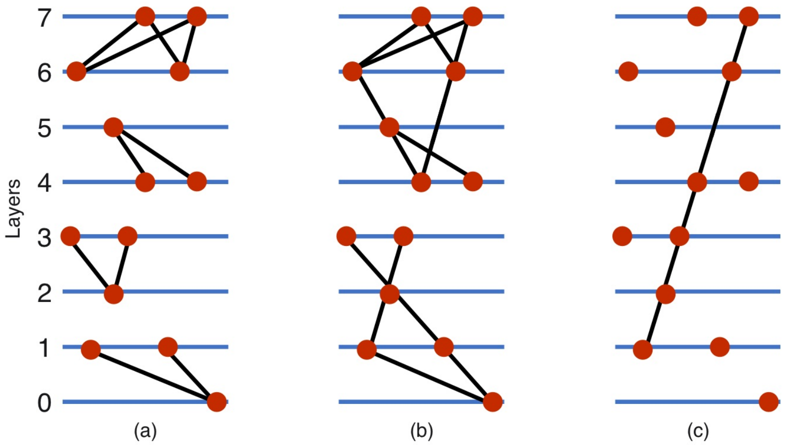

Figure 3.5: Illustration of how the algorithm finds a six-cluster track in the presence of noise. Each step is presented: (a) base case, (b) tracks which remain after one recombination, (c) identified track. Note that two-cluster tracks are present after one recombination because four layers remain to be searched and six clusters are required for a track.

of the detector. Therefore, we may wish to be able to identify tracks of particles which appear on only six or seven of the eight micromegas layers. This can be achieved using a small modification to the algorithm. The division stage will go one step further to single layers where single-cluster tracks are created. At each recombination step, the algorithm considers how many layers are needed to form a particle track, and how many layers remain to be seen in future recombinations. If a given sub-track could surpass the minimum length of a track using other sub-tracks which have yet to be seen, then it is carried over to the next step even if it doesn't immediately connect with an adjacent sub-track. After the final recombination, this leaves a straight particle track which passes through as many detector layers as possible. An example of this is shown in figure 3.5.

We now have an algorithm which can efficiently identify tracks of charged particles through the micromegas wedges of the New Small Wheel detector. When compared to the aforementioned brute force solution for identifying tracks of particles, this algorithm represents a significant improvement. At high noise rates, the brute force algorithm's poor performance had ground data analysis efforts to a halt. Using data from a sample run of data collection at the cosmic ray test stand, this algorithm ran 36x faster than the brute force solution. This allows for more data from the cosmic ray test stand to be analyzed in less time. The divide-and-conquer nature of the algorithm could also aid in searches for long-lived supersymmetric particles. This possibility is discussed in appendix C. In order to make substantive claims about the features of the tracks which have been identified in the micromegas detectors and the precision of the wedge, a straight line must now be more rigorously fit to the clusters which have been isolated. In the following chapter, an algorithm for accomplishing this task is presented along with a discussion of its implications for measuring the wedge's precision.

4

Particle Track Parameter Fitting

4.1 CALCULATION OF TRACK PARAMETERS

HAVING ISOLATED THE CLUSTERS which likely belong to a charged particle's track through the micromegas detectors, we may now focus our attention on statistically fitting the parameters which describe this track. In the absence of any magnetic field, as is the case at the cosmic ray test stand in

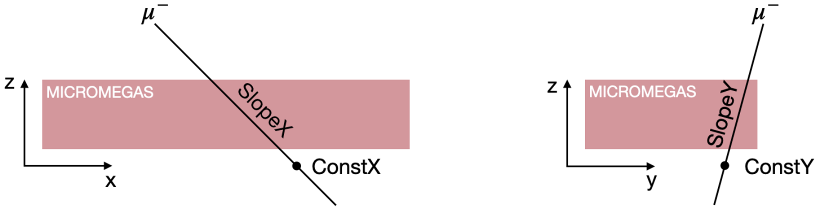

Figure 4.1: Diagram of a muon passing through a wedge of the micromegas detectors to show the definitions of SlopeX, SlopeY, ConstX, and ConstY.

building BB5, the particle would be expected to travel through the detector in a straight line. We therefore seek to fit a straight line to a small number of data points; ostensibly, this is a trivial task. The geometry of the detector and its stereo layers, however, complicates this pursuit.

A three-dimensional line can be described by four parameters. It will have a slope and an intercept in the xz-plane, and likewise in the yz-plane. These intercepts will be defined by the intersections of the line with the $z = 0$ plane in x and in y, respectively. The parameters can then be referred to as SlopeX and SlopeY for the slopes in the xz- and yz-planes, respectively, and ConstX and ConstY for the corresponding intercepts. A simple diagram showing these definitions is provided in figure 4.1. The detector does not read out a position in the yz plane, however. Strips on the stereo layers, which are offset from those on the X layers, give a measurement in x which is perturbed by the measurement in y.

https://www.overleaf.com/project/5ff611fbdb890d3722bf1602 To see how to calculate these parameters, we will work backwards and use a given configuration of the SlopeX, ConstX, SlopeY, and ConstY parameters to predict the x-position of the strip readout on a given micromegas layer. The offset of the stereo strips means that the x-positions on these layers will be altered by the y-positions of their hits, weighted by the tangent of the stereo angle. Given a layer at z-position Z_i and with stereo angle α_i, the x-position of a micromegas hit readout for a certain configuration of parameters would be:

$$x_i^{\text{pred}} = \text{ConstX} + \text{SlopeX} \cdot Z_i + (\text{ConstY} + \text{SlopeY} \cdot Z_i) \tan \alpha_i$$

We can then evaluate the χ^2 goodness of fit test[35] to determine how well these predicted hit locations fit the real data. Given an uncertainty on each measurement σ_i, which can be empirically determined for layer i as discussed in appendix A, the χ^2 goodness of fit test is computed by summing the squared difference between the predicted x-value and the real x-value for the clusters on each of the eight layers in the candidate particle track:

$$\begin{aligned} \chi^2 &= \sum_{i=0}^{7} \frac{1}{\sigma_i^2} \left(x_i^{\text{pred}} - x_i \right)^2 \\ &= \sum_{i=0}^{7} \frac{1}{\sigma_i^2} \left((\text{ConstX} + \text{SlopeX} \cdot Z_i + (\text{ConstY} + \text{SlopeY} \cdot Z_i) \tan \alpha_i) - x_i \right)^2 \end{aligned} \tag{4.1}$$

Where x_i is the x-position of the cluster center on layer i. In order to fit a particle track to data, we seek to find the parameters which minimize this quantity. Prior versions of the data analysis software for the micromegas detectors achieved this using the iterative minimizer MINUIT[22]. The χ^2 penalty function is a quadratic equation, however, so we can differentiate it with respect to each of the parameters and find a nice system of equations for its minimum. This yields a method for finding the minimum which does not require the use of an iterative minimizer, and it therefore provides a much faster algorithm for fitting the parameters to detector data. In matrix form, the system of equations for this minimum is written as:

$$\begin{pmatrix} \sum_{i=0}^{7} \frac{2}{\sigma_i^2} Z_i^2 & \sum_{i=0}^{7} \frac{2}{\sigma_i^2} Z_i & \sum_{i=0}^{7} \frac{2\tan\alpha_i}{\sigma_i^2} Z_i^2 & \sum_{i=0}^{7} \frac{2\tan\alpha_i}{\sigma_i^2} Z_i \\ \sum_{i=0}^{7} \frac{2}{\sigma_i^2} Z_i & \sum_{i=0}^{7} \frac{2}{\sigma_i^2} & \sum_{i=0}^{7} \frac{2\tan\alpha_i}{\sigma_i^2} Z_i & \sum_{i=0}^{7} \frac{2\tan\alpha_i}{\sigma_i^2} \\ \sum_{i=0}^{7} \frac{2\tan\alpha_i}{\sigma_i^2} Z_i^2 & \sum_{i=0}^{7} \frac{2\tan\alpha_i}{\sigma^2} Z_i & \sum_{i=0}^{7} \frac{2\tan^2\alpha_i}{\sigma_i^2} Z_i^2 & \sum_{i=0}^{7} \frac{2\tan^2\alpha_i}{\sigma^2} Z_i \\ \sum_{i=0}^{7} \frac{2\tan\alpha_i}{\sigma_i^2} Z_i & \sum_{i=0}^{7} \frac{2\tan\alpha_i}{\sigma_i^2} & \sum_{i=0}^{7} \frac{2\tan^2\alpha_i}{\sigma_i^2} Z_i & \sum_{i=0}^{7} \frac{2\tan^2\alpha_i}{\sigma_i^2} \end{pmatrix} \begin{pmatrix} \text{SlopeX} \\ \text{ConstX} \\ \text{SlopeY} \\ \text{ConstY} \end{pmatrix} = \begin{pmatrix} \sum_{i=0}^{7} \frac{2Z_i}{\sigma_i^2} x_i \\ \sum_{i=0}^{7} \frac{2}{\sigma_i^2} x_i \\ \sum_{i=0}^{7} \frac{2\tan\alpha_i Z_i}{\sigma_i^2} x_i \\ \sum_{i=0}^{7} \frac{2\tan\alpha_i}{\sigma_i^2} x_i \end{pmatrix}$$

From here, the system of equations can be solved by inverting the matrix on the left-hand side of the equation, and left-multiplying the column vector on the right-hand side by this inverse. It is worth noting, however, that the matrix on the left-hand side is invariant to the clusters' positions; it remains constant while the vector on the right-hand side changes. We therefore only need to compute this matrix and its inverse once. Fitting the parameters of a particle's track to data becomes as simple as constructing the column vector using cluster centers and left-multiplying it by the cached inverse matrix.

This method must also account for detector inefficiency. As discussed in the previous chapter, inefficiency will often lead to there being fewer than eight clusters to which a particle track should be fit. Equation 4.1 shows that the χ^2 penalty function is formed using the available layers, those which have a cluster in the candidate track. If certain layers are missing, then the sum must only run over the layers which do register clusters and compare the corresponding predicted *x*-positions

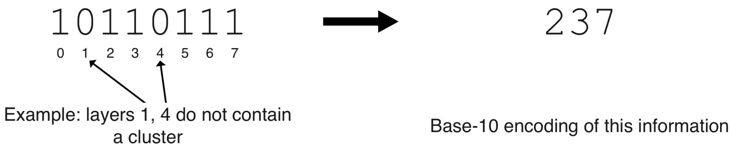

Figure 4.2: Method by which a configuration of micromegas layers is hashed.

to the actual data. Following this logic, the sums in the matrix equation will only run over these same layers, the layers which are used in the event. So, we have a general method for fitting a particle track to clusters on any configuration of micromegas layers. The matrix on the left-hand side of our matrix equation only needs to be constructed and inverted a finite number of times, once for each possible configuration of the layers. Requiring that a particle track appears on at least six of the eight layers makes:

$$\binom{8}{2} + \binom{8}{1} + \binom{8}{0} = 37$$

Possible layer configurations, and therefore 37 matrix constructions and inversions.

Each of these 37 inverted matrices can be stored in a hash table so that they are accessible in constant time when fitting a particle track. To define the hash function, the layers which register clusters in an event can be represented as an eight-bit binary string. This binary string can then be converted to base-10 and used to index the hash table which contains these inverted matrices. An example of this hashing process is shown in figure 4.2. This then defines an $\mathcal{O}(n)$ algorithm for fitting the parameters of a particle track, where n is the number clusters in the candidate track and, in reality, does not exceed eight.

When compared to iterative minimization using MINUIT, this method for fitting track parame-

	$\Delta\chi^2$/DOF	Δ SlopeX	Δ ConstX	Δ SlopeY	Δ ConstY
Mean	3.34×10^{-8}	-3.90×10^{-9}	-2.54×10^{-7}mm	-1.48×10^{-8}	-2.88×10^{-5}mm
Std. Dev.	1.78×10^{-7}	1.80×10^{-7}	2.71×10^{-5}mm	4.83×10^{-5}	6.24×10^{-3}mm

Table 4.1: Statistics on the difference between the parameters calculated by the analytical method and by MINUIT for each track. Data from 64 401 particle tracks from a single run of cosmic data collection from sector A14. Uses measurement uncertainties quoted in table B.1. Parameters computed by analytical track fitting method are subtracted from those returned by the iterative minimizer.

ters yields better fits, albeit modestly. Intuitively, this would be expected given that an iterative minimization algorithm seeks to approximate the minimum point of a function in a finite number of iterations, whereas this method provides an analytical form for the actual minimum. The differences between the parameters fit using MINUIT and those fit using this new method for a sample run of data collection at the cosmic ray test stand are quoted in table 4.1. This shows that, on average, the parameters computed by the new method result in lower χ^2/DOF values than those returned by MINUIT, indicating better fits. In addition to providing improved fits, this new method for track parameter fitting was also considerably faster than the iterative minimizer. In the same run of cosmic data collection, the analytical method fit particle tracks 25x faster than MINUIT.

4.2 Determination of Track Parameter Uncertainties

The most important contribution of this new track parameter fitting algorithm is its ability to give more rigorous quotes of the uncertainties on the parameters it computes. Understanding the uncertainties on measurements made by the detector is imperative for ensuring that it meets the precision requirements described in its Technical Design Report[23]. MINUIT computes the error matrix for these four parameters by returning the inverse of the Hessian matrix[22]. MINUIT forms this Hessian matrix by estimating second derivatives in the four-dimensional parameter space by testing the effect of making small perturbations to parameters on the given penalty (χ^2) function[22]. However, the small offset of stereo strips means that any change in the ConstY or SlopeY parameters will be weighted by a factor of $\tan \pm 1.5^\circ \approx \pm 0.026$. This complicates MINUIT's estimation of uncertainty in y in a reasonable number of iterations. To improve upon this, an analytical form for these uncertainties can be computed.

The Hessian matrix for a general function is defined to contain the partial derivatives of that function with respect to each of its variables:

$$\mathbf{H} = \begin{pmatrix} \frac{\partial\chi^2}{\partial \mathrm{SlopeX}^2} & \frac{\partial\chi^2}{\partial \mathrm{SlopeX}\partial \mathrm{ConstX}} & \frac{\partial\chi^2}{\partial \mathrm{SlopeX}\partial \mathrm{SlopeY}} & \frac{\partial\chi^2}{\partial \mathrm{SlopeX}\partial \mathrm{ConstY}} \\ \frac{\partial\chi^2}{\partial \mathrm{ConstXSlopeX}} & \frac{\partial\chi^2}{\partial \mathrm{ConstX}^2} & \frac{\partial\chi^2}{\partial \mathrm{ConstX}\partial \mathrm{SlopeY}} & \frac{\partial\chi^2}{\partial \mathrm{ConstX}\partial \mathrm{ConstY}} \\ \frac{\partial\chi^2}{\partial \mathrm{SlopeYSlopeX}} & \frac{\partial\chi^2}{\partial \mathrm{SlopeY}\partial \mathrm{ConstX}} & \frac{\partial\chi^2}{\partial \mathrm{SlopeY}^2} & \frac{\partial\chi^2}{\partial \mathrm{SlopeY}\partial \mathrm{ConstY}} \\ \frac{\partial\chi^2}{\partial \mathrm{ConstYSlopeX}} & \frac{\partial\chi^2}{\partial \mathrm{ConstY}\partial \mathrm{ConstX}} & \frac{\partial\chi^2}{\partial \mathrm{ConstY}\partial \mathrm{SlopeY}} & \frac{\partial\chi^2}{\partial \mathrm{ConstY}^2} \end{pmatrix}$$

This can be computed for equation 4.1:

$$\mathbf{H} = \begin{pmatrix} \sum_{i=0}^{7} \frac{2Z_i^2}{\sigma_i^2} & \sum_{i=0}^{7} \frac{2Z_i}{\sigma_i^2} & \sum_{i=0}^{7} \frac{2Z_i^2 \tan\alpha_i}{\sigma_i^2} & \sum_{i=0}^{7} \frac{2Z_i \tan\alpha_i}{\sigma_i^2} \\ \sum_{i=0}^{7} \frac{2Z_i}{\sigma_i^2} & \sum_{i=0}^{7} \frac{2}{\sigma_i^2} & \sum_{i=0}^{7} \frac{2Z_i \tan\alpha_i}{\sigma_i^2} & \sum_{i=0}^{7} \frac{2\tan\alpha_i}{\sigma_i^2} \\ \sum_{i=0}^{7} \frac{2Z_i^2 \tan\alpha_i}{\sigma_i^2} & \sum_{i=0}^{7} \frac{2Z_i \tan\alpha_i}{\sigma_i^2} & \sum_{i=0}^{7} \frac{2Z_i^2 \tan^2\alpha_i}{\sigma_i^2} & \sum_{i=0}^{7} \frac{2Z_i \tan^2\alpha_i}{\sigma_i^2} \\ \sum_{i=0}^{7} \frac{2Z_i \tan\alpha_i}{\sigma_i^2} & \sum_{i=0}^{7} \frac{2\tan\alpha_i}{\sigma_i^2} & \sum_{i=0}^{7} \frac{2Z_i \tan^2\alpha_i}{\sigma_i^2} & \sum_{i=0}^{7} \frac{2\tan^2\alpha_i}{\sigma_i^2} \end{pmatrix}$$

Analyzing the diagonal elements of the inverse of this matrix then gives a measure of the statisti-

	$\Delta\ \sigma^2_{\text{SlopeX}}$	$\Delta\ \sigma^2_{\text{ConstX}}$	$\Delta\ \sigma^2_{\text{SlopeY}}$	$\Delta\ \sigma^2_{\text{ConstY}}$
Mean	1.41×10^{-5}	$2.37\times10^{-1}\text{mm}^2$	4.95×10^{-1}	$8.122\times10^{3}\text{mm}^2$
Std. Dev.	2.97×10^{-6}	$7.60\times10^{-2}\text{mm}^2$	1.42	$2.83\times10^{4}\text{mm}^2$

Table 4.2: Statistics on the difference between the parameter uncertainties calculated by the analytical method and by MINUIT for each track. Data from 64 401 particle tracks from a single run of cosmic data collection from sector A14. Uses measurement uncertainties quoted in table B.1. Parameter uncertainties computed by analytical track fitting method are subtracted from those returned by the iterative minimizer.

cal uncertainty on each of the parameters. Notably, any dependence on the cluster positions has vanished. Intuitively, this means that uncertainty on the parameters depends only on the configuration of detector layers used to track the particle. Table 4.2 compares these quotes of uncertainty to those returned by MINUIT for the same cosmic run of data collection used in table 4.1. As expected, the values given for SlopeY and ConstY are, on average, radically different from what had been returned by MINUIT. This shows a key drawback of MINUIT: it is unable to effectively quote uncertainties on parameters in the imprecise coordinate. Using this new analytical form, we have an improved method for evaluating the precision of the reconstruction of a given particle's trajectory. Values for these uncertainties for each configuration of at least six layers are given in appendix B.

It should be noted that this calculation of the Hessian matrix is sensitive to the z-positions of layers. By convention, all particle track parameters are quoted using a $z = 0$ position set to be 13.804 mm below the bottom layer of the micromegas wedge at the cosmic ray test stand. Despite the symmetry of the detector in z about a midpoint between layers 3 and 4, this gives more weight to certain layers due to their increased lever arm in computing the xz and yz intercepts of a given particle track. Setting $z = 0$ to the midpoint between layers 3 and 4 ameliorates this asymmetry, however this change is not presented in these figures.

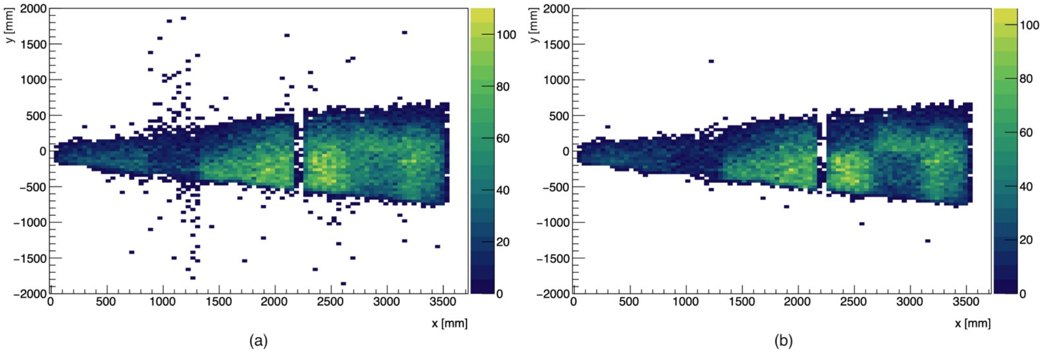

Figure 4.3: Intersection of reconstructed particle tracks in a single run of cosmic data collection with layer 7 of the micromegas wedge for sector A14. Presence of non-fiducial tracks, those which appear outside the trapezoidal detector, can be seen in (a). Cut on the uncertainty in ConstY of 1000mm^2 applied to (b).

4.3 Application to the Removal of Non-Fiducial Tracks

Equipped with improved measurements of the uncertainties on track parameters, better informed cuts can be made on candidate particle tracks in micromegas detector data. These cuts ensure that only the best tracks, those which likely originated from real muons, remain. For example, placing a cut on the uncertainty on the ConstY parameter can help reduce the presence of non-fiducial tracks. These non-fiducial tracks, those which are reconstructed to a trajectory which does not actually pass through the detector's fiducial region, could have many origins. It is possible for a charged particle's track through the detector to be particularly smeared by imprecision or multiple scattering[35], or for a noise cluster which is reasonably colinear with the particle's track to be identified by the track identification algorithm. In these cases, the straight line which best fits the data may provide a good fit with a low value of χ^2 while representing a trajectory which does not pass through the fiducial region of the detector. Clearly, this is a non-physical solution and these tracks must be removed

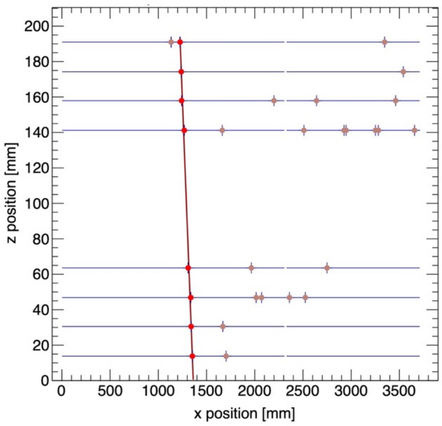

Figure 4.4: Particle track fit to identified clusters in the sample event shown in figure 3.1. Reconstructed trajectory shown as a red line passing through isolated signal clusters amidst noise clusters. Axes not to scale.

from detector data. In figure 4.3a, the presence of a significant number of these non-physical tracks, whose y-coordinates stray outside the wedge, can be seen. Figure 4.3b shows that the vast majority of these tracks can be removed using a cut on the uncertainty in ConstY of 1000mm^2. As we have shown, this corresponds to removing particle tracks which appear on a certain configuration of layers, a configuration which yields a high error on the ConstY parameter and is therefore more likely to produce non-fiducial tracks.

This completes the charged particle track reconstruction pipeline for the micromegas detectors. After isolating the clusters which are likely to belong to a particle's track, a straight line must been statistically fit to these data. This is achieved by optimizing the χ^2 goodness of fit test for a straight line through the layers of a micromegas wedge. This new method produces marginally better fits than the MINUIT iterative minimizer, however it does so 25x faster. The method also yields a more natural framework for quantifying the uncertainties on the track parameters. Using the inverse of the Hessian matrix formed by this χ^2 function allows for the detector's actual precision to be compared to what demanded by its Technical Design Report. Exploring the implications of these uncertainties allows for poor-quality, potentially non-fiducial tracks to be removed from detector data.

5

Conclusion

The New Small Wheel is a vital component of the ATLAS Experiment's phase one upgrades in preparation for run three of data collection at the LHC and in preparation for the HL-LHC upgrade. When the Collider's luminosity is increased, this new detector will be able to efficiently identify and track high-momentum muons amidst a deluge of particles and the degrading effects of the beam halo and cavern background[23]. As wedges of the New Small Wheel's micromegas detectors are constructed and tested in building BB5 of CERN's campus, efficient tools for identifying and understanding the tracks of cosmic ray muons through the detector are imperative for ensuring that it satisfies the precision requirements described in its Technical Design Report[23].

As discussed in chapter 3, a divide-and-conquer approach yields an efficient algorithm for identifying tracks of charged particles in detector data. This provides a vital improvement over the previous solution to the track identification problem, whose inefficiency had ground data analysis tools to a halt. The divide-and-conquer behavior of this algorithm, if extended to larger regions of the ATLAS Experiment, could also help search for long-lived supersymmetric particles which would disrupt the Standard Model of particle physics, as discussed in appendix C. Furthermore, as discussed in chapter 4, the parameters which describe a particle's trajectory through the micromegas detectors can be fit to an identified track in linear time using an analytical solution for the minimum point of the χ^2 goodness of fit test. In addition to providing another improvement to data analysis speed and a more robust method for parameter fitting, this algorithm also leads to a more natural process for understanding the statistical uncertainties on the particle tracks. These uncertainties help ensure that micromegas wedges are meeting the desired benchmarks for their precision, and they help remove non-fiducial tracks from detector data.

As wedges of micromegas detectors continue to be tested and installed to the New Small Wheel in preparation for its installation to the ATLAS cavern, these contributions remain vital components of the New Small Wheel team's data analysis pursuits. They allow for more data from micromegas wedges to be analyzed in less time, and with greater accuracy. Once installed to the ATLAS Experiment, the New Small Wheel is sure to play a pivotal role in the search for new physics.

Figure 5.1: New Small Wheel with several micromegas wedges installed. Source: CERN[9].

A

Determination of Hit Uncertainty

In chapter 4, an equation for the χ^2 goodness of fit test for the set of parameters which describes a charged particle's trajectory through a micromegas wedge was presented. This calculation included the variable σ_i which represents the uncertainty on the measurement of a hit on layer i. Note that this is distinct from the uncertainties on particle track parameters which were derived and represent how uncertainties at each layer convolve to give the error on a charged particle's trajectory. In order

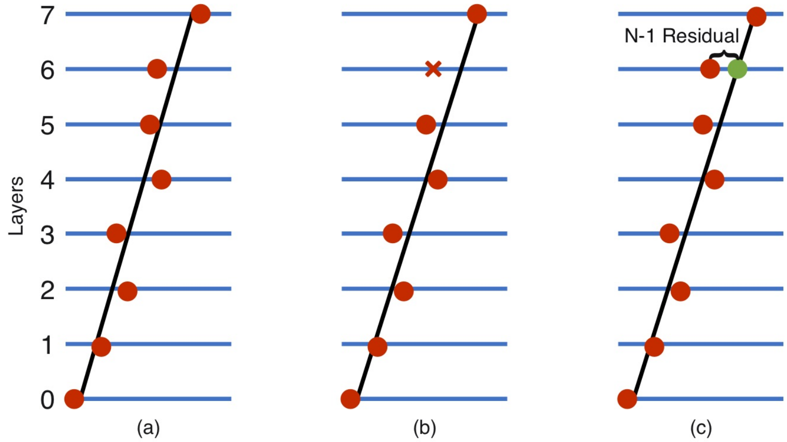

Figure A.1: Diagram showing the process of determining an $N-1$ residual for layer 6. Full eight-cluster track shown in (a), with cluster on layer 6 blinded in (b). Distance from re-fit track to original cluster in (c) is the $N-1$ residual for layer 6.

to properly compute the particle trajectory error, it is imperative that the uncertainty on a measurement made using a given layer be considered.

This uncertainty is computed using $N-1$ residuals. For each particle track, a separate track is fit with one constituent layer blinded. Given N clusters in the event and a blinded layer i, a track is fit with the $N-1$ clusters that are not on layer i. The position of a cluster at layer i is then estimated from this track, and its distance from this blinded cluster is considered. This distance is dubbed the *N−1 residual*, and looking at this residual for each layer over a large number of events in a run of cosmic data collection allows for statements to be made regarding the layers' precision. A diagram of this process is shown in figure A.1.

To compute σ_i, the distribution of $N-1$ residuals for layer i is fit to the sum of two Gaussian distributions and a uniform distribution. The uniform distribution accounts for the uniform noise

Layer	0	1	2	3	4	5	6	7
σ (mm)	0.482	0.408	0.777	0.693	0.697	0.790	0.359	0.447

Table A.1: Uncertainties on measurements made by each layer of sector A10, computed using $N-1$ residuals from 556 466 tracks.

which is distributed across a layer of the micromegas detectors while the two Gaussians nicely fit the distribution of residuals. Given weights on each Gaussian c_1, c_2, means μ_1, μ_2, and standard deviations σ_{G1}, σ_{G2}, the probability density function of this model is:

$$f(x) = c_1 \frac{1}{\sigma_{G1}\sqrt{2\pi}} \exp\left(-\frac{1}{2}\frac{(x-\mu_1)^2}{\sigma_{G1}^2}\right) + c_2 \frac{1}{\sigma_{G2}\sqrt{2\pi}} \exp\left(-\frac{1}{2}\frac{(x-\mu_2)^2}{\sigma_{G2}^2}\right) + (1-c_1-c_2)\frac{1}{x_{\max}-x_{\min}}$$

These six parameters can then be fit to the data using RooFit[33]. The distributions of the $N-1$ residuals for the layers of sector A10, as well as the fit models, are shown in figure A.2. The value of σ_i is set to the weighted combination of the two fit standard deviations for layer i:

$$\sigma_i = c_1\sigma_{G1} + c_2\sigma_{G2}$$

These values are given for sector A10 in table A.1, which uses the same run of cosmic data collection as figure A.2.

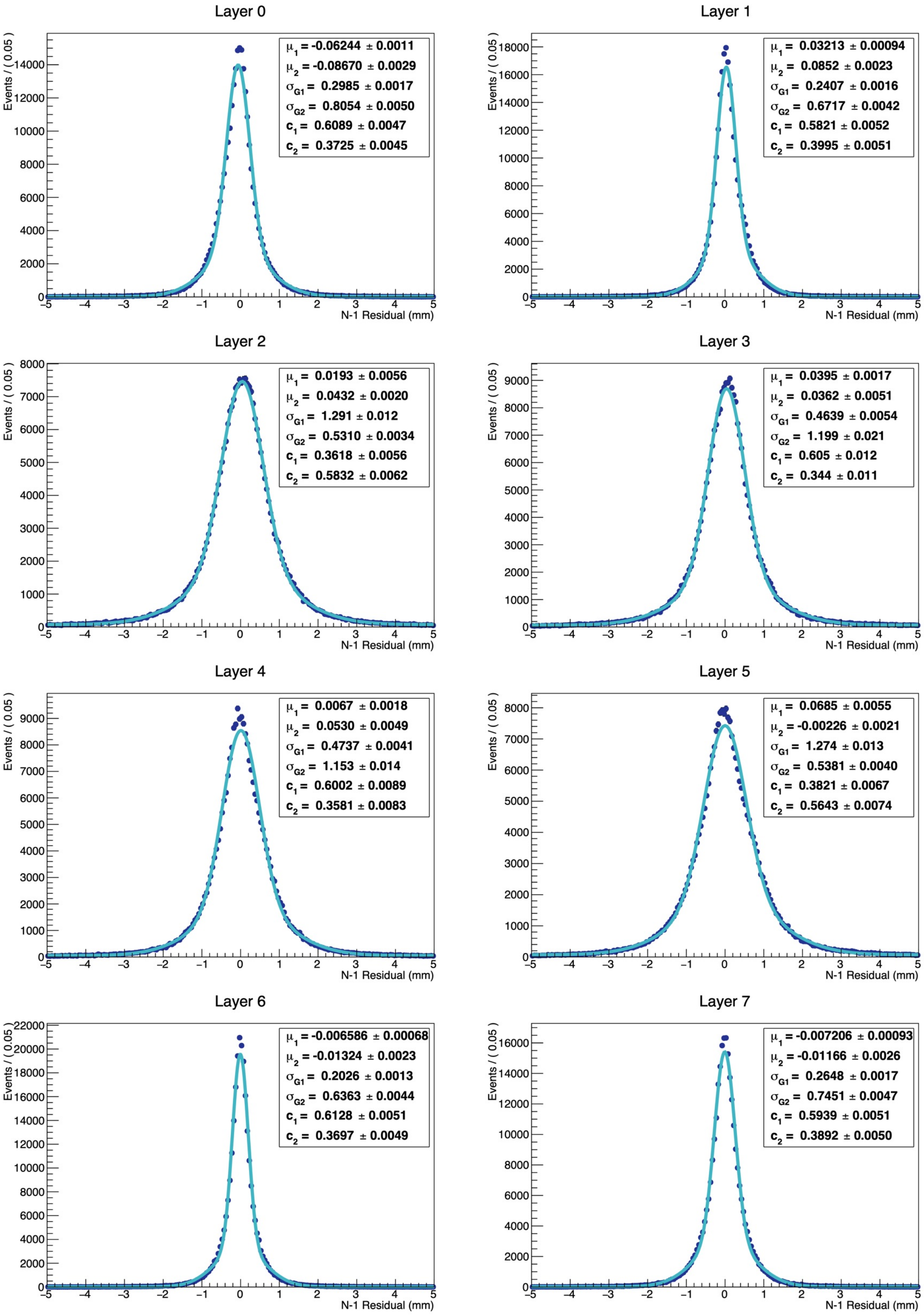

Figure A.2: Distribution of N-1 residuals for each layer of sector A10 calculated using 556 466 tracks. Fit model and parameters shown.

B

Track Parameter Uncertainties for a Single Wedge

In chapter 4, a method for determining the statistical uncertainties on the parameters which describe a charged particle's track through a wedge of micromegas detectors was presented. A central point was that these quantities depend solely on the configuration of layers used to record the track.

Layer	0	1	2	3	4	5	6	7
σ (mm)	0.36	0.36	0.52	0.65	0.52	0.65	0.36	0.36

Table B.1: Hit uncertainties used for calculations of track parameter uncertainties.

Presented here are the uncertainties on these parameters for all possible configurations of at least six out of the eight layers of a wedge, sorted in order of layer configuration frequency from a sample run of data collection at the cosmic ray test stand. This run of data collection includes 556 466 tracks from sector A10. Layer configurations are listed using the same hashing method as presented in figure 4.2. The measurement uncertainties used are given in table B.1.

Layers	Frequency	σ^2_{SlopeX}	σ^2_{ConstX} (mm^2)	σ^2_{SlopeY}	σ^2_{ConstY} (mm^2)
11111111	0.6838	2.21×10^{-6}	0.03525	0.02659	333.9
11110111	0.0465	2.35×10^{-6}	0.03535	0.04273	370.9
11101111	0.0433	2.34×10^{-6}	0.04227	0.03355	516.1
11011111	0.0413	2.39×10^{-6}	0.04187	0.06213	1058.
01111111	0.0296	3.30×10^{-6}	0.06438	0.02688	340.5
10111111	0.0279	2.82×10^{-6}	0.05463	0.02679	338.6
11111011	0.0228	2.39×10^{-6}	0.03527	0.04323	390.9
11111110	0.0192	3.26×10^{-6}	0.03709	0.02659	333.9
11111101	0.0171	2.80×10^{-6}	0.03570	0.02659	334.0
00111111	0.0074	7.50×10^{-6}	0.18670	0.02812	369.4
01011111	0.0056	4.15×10^{-6}	0.09116	0.06624	1139.
11111100	0.0042	7.09×10^{-6}	0.04157	0.02659	334.4
10110111	0.0041	2.91×10^{-6}	0.05526	0.04350	379.0
11010111	0.0041	2.49×10^{-6}	0.04231	0.07287	1065.
11001111	0.0040	2.49×10^{-6}	0.04231	2.25800	49600
11110011	0.0033	2.49×10^{-6}	0.04231	2.25800	6666.
11100111	0.0028	2.49×10^{-6}	0.04231	0.04862	545.0
01101111	0.0026	4.07×10^{-6}	0.09365	0.03682	598.2
10011111	0.0024	3.36×10^{-6}	0.07316	0.06486	1111.
01110111	0.0023	3.38×10^{-6}	0.06497	0.04348	380.4
11011011	0.0022	2.49×10^{-6}	0.04231	0.09958	1322.
10101111	0.0021	3.29×10^{-6}	0.07513	0.03577	572.4
11110101	0.0020	3.30×10^{-6}	0.03570	0.04540	378.9
11011110	0.0019	3.44×10^{-6}	0.04370	0.06213	1058.
11110110	0.0019	4.08×10^{-6}	0.03718	0.04637	380.6
11101011	0.0016	2.49×10^{-6}	0.04231	0.04794	552.0
11011101	0.0015	2.96×10^{-6}	0.04220	0.06216	1058.
11101110	0.0015	3.34×10^{-6}	0.04359	0.03359	517.7
10111011	0.0015	2.98×10^{-6}	0.05463	0.04330	394.2
11101101	0.0015	2.88×10^{-6}	0.04243	0.03365	519.3
11111010	0.0014	4.15×10^{-6}	0.03767	0.04667	401.3
01111011	0.0013	3.48×10^{-6}	0.06439	0.04347	397.1
11111001	0.0013	3.36×10^{-6}	0.03585	0.04538	396.6
01111110	0.0012	4.74×10^{-6}	0.06926	0.02689	340.5
10111110	0.0011	3.98×10^{-6}	0.05722	0.02679	338.6
10111101	0.0009	3.41×10^{-6}	0.05501	0.02679	338.8
01111101	0.0009	3.99×10^{-6}	0.06533	0.02688	340.6

Table B.2: Track parameter uncertainties sorted by layer configuration frequency from a sample run of cosmic data collection using sector A10.

C

Further Application to Disappearing-Track Studies

In chapter 3, an algorithm for identifying tracks of particles in micromegas detector data was presented. Central to this algorithm's performance was its divide-and-conquer nature. By dividing the eight layers of the detector into smaller groups, it identified tracks of particles which appeared on subsets of the detector's layers. The algorithm then attempted to stitch these sub-tracks together to create longer tracks that are more likely to have originated from an ionizing particle such as a muon. A simple tweak to the algorithm, however, could allow it to return the shorter sub-tracks which do not connect to sub-tracks in other sets of layers. Though these sub-tracks would not be very interesting in the context of data from the New Small Wheel, they could aid in the search for long-lived supersymmetric particles in other regions of the ATLAS Experiment.

Supersymmetry is a proposed extension of the Standard Model of particle physics that hypothesizes the existence of a corresponding boson to each fermion, and a corresponding fermion to each boson[35]. Notably, supersymmetric theories provide an intriguing solution for several of the mysteries of particle physics. Supersymmetry could lead to the unification of quantum mechanics with gravity[11], and it could describe the nature of the dark matter which makes up the vast majority of our universe[1]. Despite its exciting potential, however, experimental evidence for supersymmetry has not yet confirmed its validity[25]. Nonetheless, searches for proof of a variety of supersymmetric theories continue, and future particle physics experiments are designed with supersymmetry in mind[3].

The pixel detectors, which are the inner-most set of detectors surrounding the interaction point of the ATLAS Experiment[17], provide an interesting signal region for the production of certain theorized supersymmetric particles. Roughly 80 million pixels of doped silicon provide coverage extending to $\approx$15 cm from the beam line before another set of strip silicon detectors, dubbed the semiconductor tracker (SCT), provide coverage beginning at $\approx$30 cm from the beam line[17], as shown in figure C.1. This means that a charged particle which decays between 15 cm and 30 cm

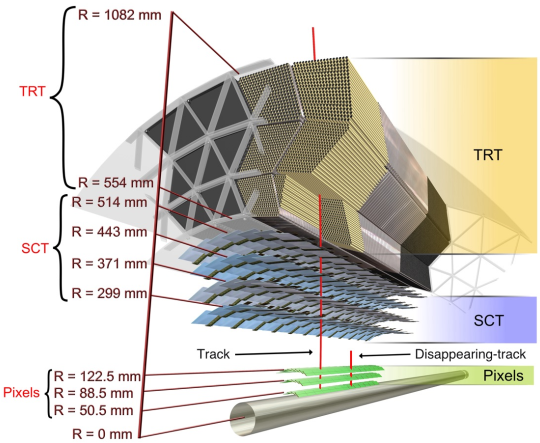

Figure C.1: Schematic of the ATLAS Inner Detector with the positions of the pixel detectors shown. Note that a fourth layer of pixel detectors at $R = 33$ mm was installed prior to the second run of data collection[30]. A disappearing-track, which does not extend into the SCT or TRT, is shown. Source: CERN[28].

from the interaction point would leave a track in only one set of detectors, the pixel detectors. This 'disappearing-track' would be difficult to isolate from noise given that the pixel detectors have only four layers, however it could be a characteristic signature of a certain kind of long-lived supersymmetric particle. Prior analyses have searched for one such exotic particle, the chargino, in the existing data of 36.1 fb^{-1} of *pp* collisions at $\sqrt{s} = 13$ TeV without success[1]. Future searches, however, such as those using data from the forthcoming High-Luminosity Large Hadron Collider, could use a similar principle to what is outlined in chapter 3 to locate disappearing-tracks in parallel with the location of standard tracks.

The long-lived chargino particle, a charged mass eigenstate of the supersymmetric W boson, is believed to decay into a pion and a neutralino as shown in figure C.2[1]. This pion would likely have a low momentum and its track would be unlikely to be reconstructed, while the neutralino would not ionize any of the inner detectors[1]. A disappearing-track through the pixel detectors could therefore

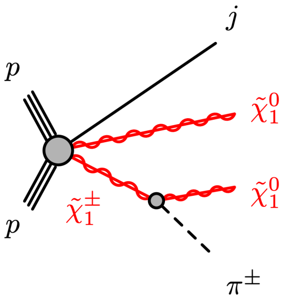

Figure C.2: Diagram showing the decay of a chargino $\left(\tilde{\chi}_1^\pm\right)$ into a neutralino $\left(\tilde{\chi}_1^0\right)$ and a pion $\left(\pi^\pm\right)$ following a pp collision. Source: ATLAS Collaboration[1].

be the only experimental evidence of chargino production. Prior searches for this long-lived supersymmetric particle have placed cuts on disappearing-track events to discriminate against known Standard Model phenomena[1]. By requiring that candidate events have missing energy in the transverse direction, E_T^{miss}, in excess of 140 GeV, for example, disappearing-tracks can be separated from jets[1]. Future studies, however, may need additional tools. The change in the energy deposited by the particle on detector layers as it travels through the inner detector, its dE/dx, could be one of those tools.

A particle's dE/dx is known to be useful for identifying its species[6]. An analytical form for the dE/dx of a general particle as it passes through material was found by Hans Bethe in 1930[35]:

$$\left\langle -\frac{dE}{dx} \right\rangle = Kz^2 \frac{Z}{A} \frac{1}{\beta^2} \left(\frac{1}{2} \ln \frac{2m_e c^2 \beta^2 \gamma^2 W_{\text{max}}}{I^2} - \beta^2 - \frac{\delta(\beta\gamma)}{2} \right)$$

For $K = 4\pi N_A r_e^2 m_e c^2 = 0.307075 \text{ MeV mol}^{-1} \text{ cm}^2$, incident particle of charge z, material of atomic number Z and mass A, mean excitation energy I, collision energy transfer to electron W, and density effect correction $\delta(\beta\gamma)$[35]. Analyzing this quantity over a range of values for $\beta\gamma = p/Mc$

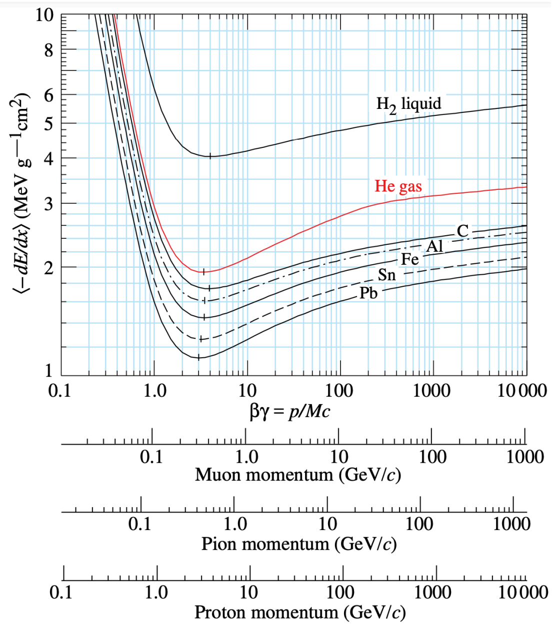

Figure C.3: Curves showing the dE/dx of various elements as they pass through a bubble chamber. Source: PDG[35].

gives rise to a distinctive curve. Figure C.3 shows examples of these curves for various elements, showing how the dE/dx of a particle over a range of values of $\beta\gamma$ can be used to identify the particle. In the low-$\beta\gamma$ region, where these curves separate, the dE/dx of a particle could tell of its species. Analyzing Monte Carlo data of chargino-producing events shows that a cut on dE/dx could aid future searches for the chargino particle in LHC data.

Disappearing-track-producing events can be identified in both signal and background Monte Carlo data. Signal Monte Carlo data refers to the simulated production and decay of long-lived chargino particles with a given mass and proper lifetime. As these particles travel away from a simulated beam crossing, their interactions with detectors is estimated so that their signature in the ATLAS Experiment's detectors can be predicted. Background Monte Carlo data refers to simula-

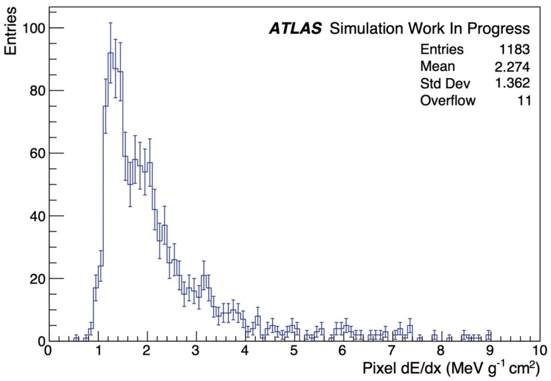

Figure C.4: Distribution of dE/dx as measured by the pixel detectors of disappearing-tracks in 10 000 simulated $\tilde{\chi}_1^{\pm}$-producing events with $m = 500$ GeV and $\tau = 1.0$ ns.

tions of the processes which could leave similar disappearing-track signatures, which are not produced by charginos, in the ATLAS Experiment. The background sources for a dE/dx-based search for disappearing-track charginos are not fully known. Previous disappearing-track searches for the chargino, however, have identified $t\bar{t}$ production and $W +$ jet events as key background processes[1]. Analyzing the distribution of the dE/dx of simulated signal and background events could motivate establishing a cut on this quantity to aid in the isolation of long-lived chargino particles during future searches.

To investigate this claim, the distribution of the dE/dx, as measured by the pixel detectors, of simulated signal and background events has been examined. Each Monte Carlo sample used in this pursuit includes 10 000 events which were subjected to selection criteria motivated by previous searches for disappearing-track charginos[1]. Disappearing-tracks were identified as tracks produced in the Experiment's pixel detectors. They were required to have a hit on each of the pixel detector's four layers, and none in the semiconductor tracker (SCT). Candidate disappearing-tracks were also

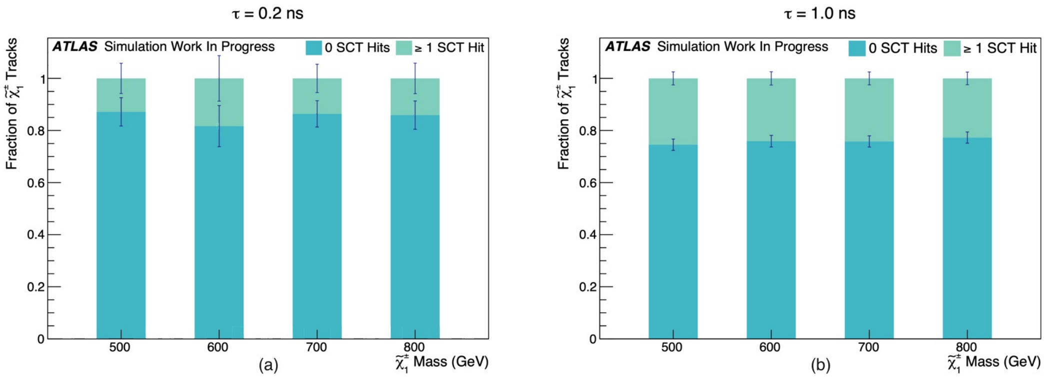

τ = 0.2 ns

τ = 1.0 ns

(a)

(b)

Figure C.5: Fraction of signal events which only produce hits in the pixel detectors compared with those which also produce at least one hit in the SCT for charginos with m = 500, 600, 700, 800 GeV. Charginos with τ = 0.2 ns shown in (a), τ = 1.0 ns shown in (b). Produced using Monte Carlo samples listed in table C.2

required to have $|\eta| < 1.8$ in order to confine the search to the barrel region of the pixel detectors, as well as a transverse momentum, p_T, in excess of 20 GeV. Table C.1 lists the number of truth-match disappearing-tracks which survived these cuts. Figure C.4 shows the distribution of the dE/dx of the truth-matched disappearing-tracks which met these criteria in a sample of chargino-producing events with $m = 500$ GeV and $\tau = 0.2$ ns. Truth-matching refers to the process by which a track in Monte Carlo data is confirmed to have originated from a given simulated particle. In this scenario, a truth-matched track refers to one which originated from a simulated chargino.

Figure C.6 shows the fraction of simulated chargino-matched disappearing-track events which would be retained with various cuts on dE/dx alongside the disappearing-tracks that are associated with $t\bar{t}$ and $W+$ jet events which would be removed. This includes $t\bar{t}$ producing events with and without jets, and $W+$ jet events in which the W boson decays as $W \rightarrow e\nu$. Chargino masses in excess of what has been excluded in prior searches for a chargino with proper lifetime of 0.2 ns have been investigated[1]. Charginos with the same mass and a proper lifetime of 1.0 ns have also been

τ	0.2 ns				1.0 ns			
Mass	500 GeV	600 GeV	700 GeV	800 GeV	500 GeV	600 GeV	700 GeV	800 GeV
Sample ID	448302	448304	448394	448396	448494	448496	448498	448404
$n_{\text{Disappearing-Tracks}}$	258	107	292	250	1 183	1 159	1 241	1 303

Table C.1: Monte Carlo sample ID and number of truth-matched disappearing-tracks which passed the cuts on η and p_T for various masses and proper lifetimes of charginos, out of 10 000 events per sample.

evaluated. These particles are likely to travel further into the ATLAS Experiment's inner detector, and potentially interact with its SCT. Figure C.5 shows that a significant number of these simulated charginos with $\tau = 1.0$ ns interacted with the SCT. Some signal in disappearing-track searches for charginos of this lifetime would therefore be lost to charginos which travel further into the inner detector. Conversely, dE/dx searches that restrict themselves to tracks which extend into the SCT may be neglecting a significant number of charginos which decay prior to the SCT. Figure C.6 shows that a dE/dx cut may still be useful in this signal region.

As shown in figure C.6, a dE/dx lower bound of 1.79 MeV g^{-1} cm^2 would remove in excess of 80% of W+ jet events, and in excess of 90% of $t\bar{t}$-producing events. This cut would also retain 22.1% of the truth-matched disappearing-tracks for charginos with a mass of 500 GeV and $\tau = 0.2$ ns. The fraction of truth-matched disappearing-tracks which are retained by this cut then increases with the mass and proper lifetime of the chargino. For charginos with a mass of 800 GeV and $\tau = 1.0$ ns, this fraction increases to 64.6%. Figure C.5 shows that searches for this type of chargino which are restricted to tracks that extend into the SCT may be neglecting more than 75% of the particles. The disappearing-track region, therefore, may provide an exciting extension to the signal regions of future dE/dx searches for long-lived supersymmetric charginos.

Moving forward, more work is needed in order to better understand the background processes which would be present in a disappearing-track search for the chargino particle using dE/dx methods. Though figure C.6 shows that a dE/dx cut could effectively separate charginos from disappearing-tracks produced by $t\bar{t}$ production and $W+$ jet events, it is possible that there are other sources which have not been considered. Nonetheless, disappearing-tracks pose an intriguing signal region for dE/dx studies as current searches for the chargino which are restricted to tracks which extend through the ATLAS Experiment's SCT could be neglecting a significant amount of signal. Future searches could use a method similar to the track identification algorithm presented in chapter 3, which was originally designed for data from the micromegas detectors of the New Small Wheel, to locate these disappearing-tracks alongside the identification of full inner detector tracks.

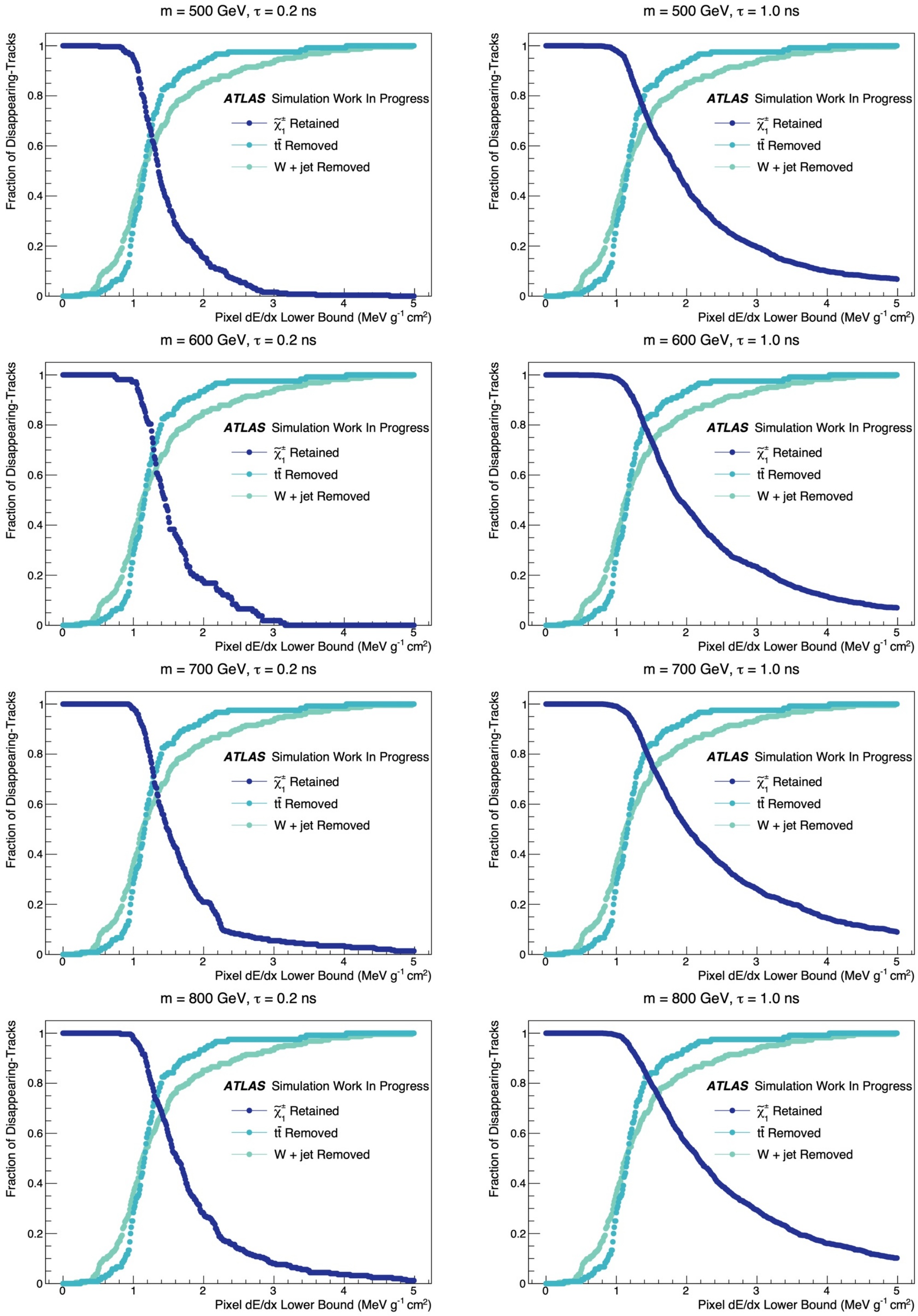

Figure C.6: Fraction of signal events which are retained and background events which are removed with various cuts on pixel dE/dx. Produced using Monte Carlo samples listed in table C.2

Sample
mc16_13TeV.448302.MGPy8EG_A14N23LO_mAMSB_C1N1_5000_172600_LL0p2_MET60.deriv.DAOD_SUSY6.e6962_s3353_r9364_p3877
mc16_13TeV.448494.MGPy8EG_A14N23LO_mAMSB_C1N1_5000_172600_LL1p0_MET60.deriv.DAOD_SUSY6.e7157_s3353_r9364_p3877
mc16_13TeV.448304.MGPy8EG_A14N23LO_mAMSB_C1N1_5000_208000_LL0p2_MET60.deriv.DAOD_SUSY6.e6962_s3353_r9364_p3877
mc16_13TeV.448496.MGPy8EG_A14N23LO_mAMSB_C1N1_5000_208000_LL1p0_MET60.deriv.DAOD_SUSY6.e7157_s3353_r9364_p3877
mc16_13TeV.448394.MGPy8EG_A14N23LO_mAMSB_C1N1_5000_243800_LL0p2_MET60.deriv.DAOD_SUSY6.e7157_s3353_r9364_p3877
mc16_13TeV.448498.MGPy8EG_A14N23LO_mAMSB_C1N1_5000_243800_LL1p0_MET60.deriv.DAOD_SUSY6.e7157_s3353_r9364_p3877
mc16_13TeV.448396.MGPy8EG_A14N23LO_mAMSB_C1N1_5000_279600_LL0p2_MET60.deriv.DAOD_SUSY6.e7157_s3353_r9364_p3877
mc16_13TeV.448404.MGPy8EG_A14N23LO_mAMSB_C1N1_5000_279600_LL1p0_MET60.deriv.DAOD_SUSY6.e7157_s3353_r9364_p3877
mc16_13TeV.410470.PhPy8EG_A14_ttbar_hdamp258p75_nonallhad.deriv.DAOD_SUSY6.e6337_s3126_r9364_p3736
mc16_13TeV.410471.PhPy8EG_A14_ttbar_hdamp258p75_allhad.deriv.DAOD_SUSY6.e6337_s3126_r9364_p3736
mc16_13TeV.364170.Sherpa_221_NNPDF30NNLO_Wenu_MAXHTPTV0_70_CVetoBVeto.deriv.DAOD_SUSY6.e5340_s3126_r9364_p3736
mc16_13TeV.364172.Sherpa_221_NNPDF30NNLO_Wenu_MAXHTPTV0_70_BFilter.deriv.DAOD_SUSY6.e5340_s3126_r9364_p3736
mc16_13TeV.364171.Sherpa_221_NNPDF30NNLO_Wenu_MAXHTPTV0_70_CFilterBVeto.deriv.DAOD_SUSY6.e5340_s3126_r9364_p3736

Table C.2: Monte Carlo samples used. Sections provide $\tilde{\chi}_1^{\pm}$, $t\bar{t}$, and W + jet events, respectively.

References

[1] Aaboud, M., Aad, G., Abbott, B., Abdinov, O., Abeloos, B., Abidi, S. H., AbouZeid, O. S., Abraham, N. L., Abramowicz, H., & et al. (2018). Search for long-lived charginos based on a disappearing-track signature in pp collisions at $\sqrt{s} = 13$ TeV with the ATLAS detector. *Journal of High Energy Physics*, 2018(6).

[2] Aad, G., Abajyan, T., Abbott, B., Abdallah, J., Abdel Khalek, S., Abdelalim, A., Abdinov, O., Aben, R., Abi, B., Abolins, M., & et al. (2012). Observation of a new particle in the search for the Standard Model Higgs boson with the ATLAS detector at the LHC. *Physics Letters B*, 716(1), 1–29.

[3] Abada, A., Abbrescia, M., AbdusSalam, S. S., Abdyukhanov, I., Abelleira Fernandez, J., Abramov, A., Aburaia, M., Acar, A. O., Adzic, P. R., Agrawal, P., & et. al. (2019). FCC Physics Opportunities. *The European Physical Journal C*, 79(6), 474.

[4] ATLAS Collaboration (1994). *ATLAS: technical proposal for a general-purpose pp experiment at the Large Hadron Collider at CERN*. LHC Tech. Proposal. Geneva: CERN.

[5] ATLAS Collaboration (1997). *ATLAS muon spectrometer: Technical Design Report*. Technical design report. ATLAS. Geneva: CERN.

[6] ATLAS Collaboration (2011). *dE/dx measurement in the ATLAS Pixel Detector and its use for particle identification*. Technical Report ATLAS-CONF-2011-016, CERN, Geneva.

[7] ATLAS Collaboration (2012). *Physics at a High-Luminosity LHC with ATLAS (Update)*. Technical Report ATL-PHYS-PUB-2012-004, CERN, Geneva.

[8] Brice, M. (2008). Aerial View of the CERN taken in 2008.

[9] Brice, M. (2021). The ATLAS New Small Wheels (NSW) detectors. General Photo.

[10] Brumfiel, G. (2008). Particle physics: The race to break the standard model. *Nature*, 455, 156–159.

[11] Chamseddine, A. H., Arnowitt, R., & Nath, P. (2001). Supergravity unification. *Nuclear Physics B - Proceedings Supplements*, 101(1), 145–153.

[12] European Organization for Nuclear Research (2019). A new schedule for the LHC and its successor. *CERN*.

[13] European Organization for Nuclear Research (2021a). Facts and figures about the LHC. *CERN*.

[14] European Organization for Nuclear Research (2021b). High-Luminosity LHC. *CERN*.

[15] Evans, R. (2008). Scientists send first beam round atom-smasher. *Thomson Reuters*, (PRESSCUT-V-2009-4250), No pagination.

[16] Giomataris, I., Rebourgeard, P. C., Robert, J. P., & Charpak, G. (1995). Micromegas: a high-granularity position-sensitive gaseous detector for high particle-flux environments. *Nucl. Instrum. Methods Phys. Res., A*, 376(DAPNIA-SED-95-04. 1), 29–35. 20 p.

[17] Green, D. (2010). *At the Leading Edge: The ATLAS and CMS LHC Experiments*. World Scientific.

[18] Griffiths, D. (2008). *Introduction to Elementary Particles*. Physics textbook. Wiley.

[19] Hastie, T., Tibshirani, R., & Friedman, J. (2013). *The Elements of Statistical Learning: Data Mining, Inference, and Prediction*. Springer Series in Statistics. Springer New York.

[20] Higgs, P. W. (1964). Broken symmetries and the masses of gauge bosons. *Phys. Rev. Lett.*, 13, 508–509.

[21] Izzo, V. (2020). *ATLAS Upgrades*. Technical Report ATL-UPGRADE-PROC-2020-001, CERN, Geneva.

[22] James, F. & Roos, M. (1975). MINUIT: a system for function minimization and analysis of the parameter errors and corrections. *Comput. Phys. Commun.*, 10(CERN-DD-75-20), 343–367. 38 p.

[23] Kawamoto, T., Vlachos, S., Pontecorvo, L., Dubbert, J., Mikenberg, G., Iengo, P., Dallapiccola, C., Amelung, C., Levinson, L., Richter, R., & Lellouch, D. (2013). *New Small Wheel Technical Design Report*. Technical Report CERN-LHCC-2013-006. ATLAS-TDR-020. ATLAS New Small Wheel Technical Design Report.

[24] Livan, M. (1996). Monitored drift tubes in ATLAS. *Nuclear Instruments and Methods in Physics Research Section A: Accelerators, Spectrometers, Detectors and Associated Equipment*, 384(1), 214–218. BEAUTY '96.

[25] Lykken, J. & Spiropulu, M. (2014). Supersymmetry and the crisis in physics.

[26] Milgrom, M. (2002). Does dark matter really exist? *Scientific American*, 287(2), 42–52.

[27] Nagai, K. (1996). Thin gap chambers in atlas. *Nuclear Instruments and Methods in Physics Research Section A: Accelerators, Spectrometers, Detectors and Associated Equipment*, 384(1), 219–221. BEAUTY '96.

[28] Pequenao, J. (2008a). Computer generated image of the ATLAS inner detector.

[29] Pequenao, J. (2008b). Computer generated image of the whole ATLAS detector.

[30] Pernegger, H. (2015). *The Pixel Detector of the ATLAS Experiment for LHC Run-2*. Technical Report ATL-INDET-PROC-2015-001. 06, CERN, Geneva.

[31] Purcell, E. & Morin, D. (2013). *Electricity and Magnetism*. Electricity and Magnetism. Cambridge University Press.

[32] Rosso, A. D. (2015). Tracking the LHC halo. Suivre le halo du LHC à la trace. (BUL-NA-2015-065. 14/2015), 4.

[33] Verkerke, W. & Kirkby, D. (2003). The RooFit toolkit for data modeling.

[34] Ward, E. (2019). ATLAS New Small Wheels. General Photo.

[35] Zyla, P.A. et al. and Particle Data Group (2020). Review of Particle Physics. *Progress of Theoretical and Experimental Physics*, 2020(8). 083C01.